Centrosomal Enrichment and Proteasomal Degradation of SYS-1/β-catenin Requires the Microtubule Motor Dynein

Joshua W. Thompson, Maria F. Valdes Michel, Bryan T. Phillips

Abstract

The *C. elegans* Wnt/β-catenin Asymmetry (WβA) pathway utilizes asymmetric regulation of SYS-1/β-catenin and POP-1/TCF coactivators. WβA differentially regulates gene expression during cell fate decisions, specifically by asymmetric localization of determinants in mother cells to produce daughters biased towards their appropriate cell fate. Despite the induction of asymmetry, β-catenin localizes symmetrically to mitotic centrosomes in both mammals and *C. elegans*. Due to the mitosis-specific localization of SYS-1 to centrosomes and enrichment of SYS-1 at kinetochore microtubules when SYS-1 centrosomal loading is disrupted, we investigated active trafficking in SYS-1 centrosomal localization. Here, we demonstrate that trafficking by microtubule motor dynein is required to maintain SYS-1 centrosomal enrichment, by dynein RNAi-mediated decreases in SYS-1 centrosomal enrichment and by temperature-sensitive allele of the dynein heavy chain. Conversely, we observe depletion of microtubules by nocodazole treatment or RNAi of dynein-proteasome adapter ECPS-1 exhibits increased centrosomal enrichment of SYS-1. Moreover, disruptions to SYS-1 or negative regulator microtubule trafficking are sufficient to significantly exacerbate SYS-1 dependent cell fate misspecifications. We propose a model whereby retrograde microtubule-mediated trafficking enables SYS-1 enrichment at centrosomes, enhancing its eventual proteasomal degradation. These studies support the link between centrosomal localization and enhancement of proteasomal degradation, particularly for proteins not generally considered 'centrosomal'.

Keywords

Development, Wnt, β-catenin, microtubule, ECM29, dynein, proteasome, trafficking, elegans, asymmetry, cell cycle, robustness

30 **Introduction**

31 During metazoan development, cells must robustly respond to and integrate multiple signaling
32 pathways to appropriately specify and populate tissues. This is of further importance in the developing
33 embryo, where cell division rapidly alternates between S-phase and mitosis while simultaneously
34 specifying tissues and entire germ layers (Pintard and Bowerman 2019). As such, the cell's response to
35 signals and the subsequent establishment of asymmetry often begins before daughter cells are 'born'
36 via an asymmetric cell division (ACD) (Sunchu and Cabernard 2020; Juanes, 2020; Fuchs and Chen, 2013;
37 Gómez-López, Petrisch et al 2014). Among the signaling pathways utilized in development is Wnt/β-
38 catenin signaling, wherein the binding of Wnt ligands dismantlesthe Axin and APC containing destruction
39 complex . This stabilizes transcriptional co-activator β-catenin, enabling it to activate target genes with
40 activator TCF/LEF (Nusse and Clevers 2017). Wnt/β-catenin signaling is specialized in its ability to
41 regulate both polarity and proliferation – with the Wnt signal orienting and promoting expansion of
42 tissues simultaneously (Loh et al 2016).

43 Due to its role in both proliferation and polarity, Wnt/β-catenin can bewellused bythe
44 organization to pattern a stem cell niche for tissue maintenance (Pinto, Clevers et al 2003; Reilein,
45 Kalderon et al 2017). However, this function in adult tissue homeostasis also implicates dysregulation of
46 Wnt/β-catenin signaling with hyper-proliferative disease states. Throughout transduction of the Wnt
47 signal are proteins vulnerable to oncogenic mutation (Yang, yen 2011; Zhunussova, Djansugurova et al
48 2019; Liu, Thibodeau et al 2000). However, these often affect their tumorigenicity via dysregulation of
49 the pathway effector β-catenin, which can promote proliferation by over-and mis-expression of targets
50 like Cyclin D1 and cMyc or metastasis by disrupting adherens junctions (Niehrs, Acebron 2012; He,
51 Kinzler et al 1998; Shtutman, Ben-Ze'ev et al 1999; Tetsu and McCormick, 1999; Reya, Clevers 2005).).
52 The combination of these roles for β-catenin makes it an attractive target for studying tumorigenesis.

53 However, the dual functions can also lead to confounding pleiotropic phenotypes after manipulation of
54 β-catenin activity (Reya, Clevers 2005; Tejpar, Alman et al 1999; Geyer, Reis-Filho et al 2011).

55 Unlike β-catenin in the canonically described Wnt signaling pathway, *C. elegans* has distributed
56 the adhesive and signaling roles across its four β-catenins (Sawa, 2012). Here we focus specifically on
57 the *C. elegans* β-catenin SYS-1 for its role as a transcriptional co-activator in a modified version of
58 canonical Wnt signaling, the Wnt/β-catenin Asymmetry pathway(WβA) (Phillips, Kimble et al 2007).
59 Similar to canonical Wnt, the WβA pathway regulates co-activator SYS-1 (β-catenin), which modulates
60 the activity of transcription factor POP-1 (TCF) during asymmetric cell division (Baldwin and Phillips
61 2018, Lam and Phillips 2017). Mother cells undergoing a WβA-driven division polarize components of
62 the Wnt signaling pathway along the axis of the division – distributing positive regulators of a Wnt
63 response, the Frizzled receptor and downstream effector Disheveled, to the signaled pole of the cell,
64 and negative regulators, members of the β-Catenin destruction complex APC and Axin, to the unsignaled
65 pole (Baldwin and Phillips 2014; Baldwin, Phillips et al 2016; Sugioka, Sawa et al 2011; Mizumoto and
66 Sawa, 2007). Daughter cells in such a division therefore inherit Wnt signaling components that bias them
67 toward their appropriate cell fate. Contrary to its known role asymmetrically activating Wnt target
68 genes, SYS-1 (and indeed, mammalian β-catenin (Mbom, Barth et al 2014; Vora, Phillips et al 2020)),
69 unexpectedly localizes symmetrically to mother cell mitotic centrosomes (Phillips, Kimble et al 2007;
70 Huang, Lin et al 2007; Vora and Phillips 2015).

71 Previous work has demonstrated that centrosomal localization of SYS-1 in mother cells limits
72 SYS-1 levels in daughter cells in a proteasome dependent manner (Vora and Phillips 2015). Similarly,
73 differential localization of the proteasome has been shown to structurally and functionally disrupt
74 protein complexes (Baldin, Coux et al 2008; Amsterdam, Baumeister et al 1993), suggesting that the
75 regulation and localizationof protein clearance are interdependent. Proteasomal subunits have

76 specifically been shown to co-sediment with centrosomal proteins and perinuclear inclusions,
77 demonstratingthat the proteasome may be centrosomally localized (Wigley, Thomas et al 1999; Wojcik,
78 DeMartino 2003). Similarly, turnover of the SYS-1 mobile fraction at mitotic centrosomes is enhanced by
79 RPT-4 proteasomal activity (Vora and Phillips 2015). When the localization of SYS-1 to centrosomes is
80 reduced by *rsa-2(RNAi)*, resultant daughter cells retain 40% additional SYS-1 protein. Perhaps, then, the
81 centrosome is a region where SYS-1 and regulators of its degradation are concentrated to enhance SYS-1
82 regulation..

83 The directionality and temporal specificity of SYS-1 enrichment at only mitotic centrosomes
84 implied that a more active localization mechanism might be at work, as compared to a passive diffusion-
85 capture mechanism. Centrosomal SYS-1 maintains a proteasome-dependent, 100% mobile fraction,
86 which is recycled within 120 seconds, yet remains undetectable via SYS-1 fluorescence on interphase
87 centrosomes(Vora and Phillips 2015). The mechanism of such rapid and temporally specific SYS-1
88 localization is unknown. Several observations indicate that cells utilize the microtubule cytoskeleton for
89 rapid and directional localization of cargo, including: transcription factors due to neuronal injury or
90 signaling status, (Ben-Yaakov, Fainzilber et al 2012; Mikenberg, Kaltschmidt et al 2007) and endocytic
91 recycling components around the Microtubule Organizing Center (MTOC) (Horgan, Mccaffrey et al 2010)
92 or preventing pathogenic accumulation of RNA binding proteins (Deshiumaru, Tsuboi et al 2021).
93 Therefore, we hypothesized that the role of the mitotic centrosome as an MTOC could facilitate the
94 rapid transport of SYS-1 to the pericentriolar material specifically in dividing cells.

95 Accumulation of SYS-1 at an MTOC like the mitotic centrosome is most likely accomplished by
96 the minus end-directed dynein microtubule motor complex (Vora and Phillips 2015; Priyanga, Bhaka-
97 Guha et al 2021). The dynein motor is a multi-subunit complex composed of a pair of ATP-ase,
98 microtubule-binding heavy chains responsible for the force-generating steps of the motor, and a
99 variable complement of smaller light, intermediate, and accessory chains that alter cargo binding or the

100 processivity of the motor (Reck-Peterson, Carter et al 2018; Jha and Surrey 2015). The dynein motor is
101 multifunctional - it provides pulling forces, positions organelles, and can mediate rapid and conditional
102 movement of proteins and RNAs (Carminati and Stearns 1997; Woźniak, Allan et al 2009; Harada,
103 Hirokawa et al 1998; Hanz, Fainzilber et al 2003; Bullock and Ish-Horowicz 2001). For example, injured
104 rat axons have demonstrated a dynein intermediate chain-dependent nuclear localization and
105 coimmunoprecipitation of the transcription factor STAT3 to transcriptionally respond to injury (Ben-
106 Yaakov, Fainzilber et al 2012). Dynein specifically is the motor complex most often directed towards the
107 MTOC, and is known to be active during mitosis (Jha and Surrey 2015). Therefore, we focused our
108 investigation on dynein-dependent trafficking as an ideal mechanism for SYS-1 localization to the MTOC
109 mitotic centrosomes.

110 Here we demonstrate that microtubules and minus-end microtubule-mediated trafficking are
111 required for both the centrosomal recruitment and clearance of SYS-1. We evaluate the extent to which
112 SYS-1 utilizes dynein-mediated trafficking to accumulate at centrosomes by RNAi screen, and evaluate
113 the effect of long and short term disruptions to microtubule-mediated trafficking on SYS-1 localization,
114 target gene activity, and cell fate decisions.. Together, these data characterize a role for microtubule-
115 mediated trafficking in arobust response to the WβA signaling pathway by enhancing the interaction of
116 SYS-1 with negative regulators at the mitotic centrosome.

117 **Results**

118 **SYS-1 Overexpression and Centrosomal Uncoupling Increases SYS-1 Localization to Regions of Dynein**
119 **Enrichment**

120 To test the role of microtubule-mediated trafficking in SYS-1 centrosomal localization, we
121 investigated what trafficking mechanisms are necessary for SYS-1 regulation. As described above, we
122 focused on the minus-end directed cytoplasmic dynein motor complex. The dynein localization pattern

123 corresponded to that of GFP::SYS-1, localizing to centrosomal, cortical, and microtubule dense
124 kinetochore regions (Schmidt, Van den Heuvel et al 2017; Tame, Medema et al 2014). Moreover, the
125 kinetochore and cortical localization of GFP::SYS-1 was more common upon disruption of SYS-1
126 centrosomal localization by RNAi depletion of RSA-2(Fig. 1A).

127 While GFP::SYS-1 has been observed at mitotic centrosomes in many dividing cells throughout
128 development, localization to these cortical and kinetochore 'secondary' sites is uncommon
129 (accumulation at either or both of these sites occurring in 34.5% of embryos) in untreated embryos
130 (Fig.1A). Uncoupling SYS-1 protein from the centrosome by *rsa-2(RNAi)*, leads to more frequent
131 detection of SYS-1 at sites of dynein and kinesin localization (Fig. 1A). Given its comparable localization
132 to kinetochore microtubules, cortex, and the MTOC/centrosome, SYS-1 may be a cargo of the dynein or
133 kinesin microtubule motors (Vora and Phillips 2015; Vora and Phillips 2017; Ferenz, Wadsworth et al
134 2010; Schmidt, Van den Heuvel et al 2017).
135 .

136

137 **Knockdown of Dynein Complex Subunits Reduces SYS-1 Centrosomal Localization**

138 Given the observation that SYS-1 localizes to cortical and kinetochore sites that also exhibit
139 enrichment for microtubule motors, we investigated a functional role for microtubule-mediated
140 trafficking in SYS-1 localization. We began by performing an RNAi screen against components of the
141 dynein motor complex and dynein associated proteins, expanding to additional motors and known
142 microtubule-affecting proteins (Fig. S1). We assayed the centrosomal enrichment of GFP::SYS-1 in each
143 of these depletions. We expected depletion of transport proteins that play a role in SYS-1 centrosomal
144 transport to be defective in the maintenance of SYS-1 centrosomal enrichment when SYS-1 centrosomal
145 clearance was otherwise unaffected. In order to evaluate the centrosome-specific enrichment of SYS-1,

146 we considered two ways of comparing the extent of fluorescently-tagged SYS-1 localization to
147 centrosomes: 1) the centrosomal enrichment index (CEI,similar to that described in Gao, Smith et al
148 2017), the centrosomal fluorescence intensity with background cytoplasmic fluorescent intensity of the
149 surrounding cell subtracted, to control for backgrounds that may pleiotropically influence SYS-1
150 expression, and 2) the SYS-1 CEI evaluated proportionally to the enrichment factor of representative Peri
151 Centriolar Material (PCM) factor γ-tubulin (Tubulin Enrichment Index, or TEI) , to avoid false positives via
152 defects in PCM maturation (CEI/TEI) (Fig. 1B-B''). We then compared these centrosomal enrichment
153 metrics between microtubule motor depletions and established *rsa-2(RNAi)* centrosomal uncoupling
154 (Fig. 1C-C').

155 As expected, depletion of dynein subunits often resulted in pleiotropic and deleterious effects,
156 including oogenesis and early patterning defects that precluded our SYS-1 localization assay. We
157 therefore treated animals with partial RNAi knockdowns by commencing RNAi feeding 12-24 hours
158 before imaging as necessary, based on the phenotypic severity. While no treatment disrupted SYS-1
159 centrosomal levels as severely as *rsa-2(RNAi)*, we did observe several statistically significant decreases in
160 centrosomal SYS-1 enrichment (Fig. 21C – C', Fig. S1). Furthermore, while the total population of some
161 treatments displayed only an intermediate decrease in SYS-1 CEI, the distribution of SYS-1 CEI values
162 observed in dynein subunit knockdowns extends from wild-type to an *rsa-2(RNAi)*-like disruption (e.g.,
163 Fig. 2 Supplement 1). Dynein knockdown-induced decreases in SYS-1 CEI or CEI/TEI were therefore
164 masked somewhat by their broad range in phenotype and/or RNAi penetrance (Fig. 1C-C', Fig S2). Most
165 notably, *dlc-1(RNAi)* and *dylt-1(RNAi)* each exhibit a significant reduction in centrosomal SYS-1
166 localization disproportionately larger than the effect on γ-Tubulin. Loss of centrosomal SYS-1 enrichment
167 was specifically more visible in a transgene driven by the endogenous SYS-1 promoter (P_{sys-}
168 $_{1}$::VENUS::SYS-1), as compared to SYS-1 driven by the stronger *pie-1* promoter (P_{pie-1}::GFP::SYS-1) (Fid 2C-
169 C').

170 While we observed dynein-dependent decreases in SYS-1 localization, this could be because of
171 changes in the RSA-2 centrosomal scaffold, which is responsible for capturing SYS-1 at mitotic
172 centrosomes (Vora and Phillips 2015, Schlaitz, Hyman et al 2007). Depleting some dynein subunits did
173 result in a slight decrease in centrosomal GFP::RSA-2 - 16% reduction in dlc-1(RNAi) embryos and 14% in
174 dylt-1(RNAi) embryos. Embryos depleted of DLC-1 by RNAi exhibit a much more pronounced effect on
175 SYS-1 localization, with 39% and 42% reductions in Psys-1::VENUS::SYS-1 CEI and CEI/TEI, respectively.
176 DYLT-1 depletion exhibited a similar 14% decrease in CEI alone, but a 39% decrease in CEI/TEI. Both
177 results suggest that tagged SYS-1 is disproportionately removed from centrosomes in these dynein
178 subunit knockdowns (Fig. S3)

179 These data suggest that dynein does have a role in the localization of SYS-1 to centrosomes, but
180 redundancy between components of the dynein motor or between the dynein motor and other
181 trafficking processes may limit the effect any one subunit has on SYS-1 localization. Alternately,
182 variability of RNAi efficacy may have resulted in incomplete depletion of SYS-1 relevant dynein subunits.
183 Similarly, the pleiotropic effects of dynein depletion may also have precluded our ability to measure
184 their effects on SYS-1 localization, leading to the evaluation of only partial knockdowns. In order to
185 address these issues, we investigated the role of the dynein motor in SYS-1 localization at a more precise
186 temporal resolution via conditional dynein disruption.

187 **Temporally Restricted Dynein Loss of Function Reveals Dynein Requirement for Centrosomal SYS-1**
188 **Accumulation.**

189 While the results of our screen demonstrate that dynein knockdown significantly reduces SYS-1
190 centrosomal enrichment, rare individuals exhibiting *rsa-2(RNAi)*-like loss of centrosomal SYS-1
191 accumulation, we were unable to completely recreate a population exhibiting consistently severe
192 disruption to SYS-1 CEI. To distinguish between functional redundancies limiting the effects of dynein

193 depletion and the confounding deleterious effects described above, we utilized a temperature sensitive
194 allele of the cytoplasmic dynein heavy chain, *dhc-1(or195ts),* to conditionally inactivate the cytoplasmic
195 dynein heavy chain. This allele, identified in the Bowerman lab at the University of Oregon, introduces a
196 lesion to the microtubule binding stalk of DHC-1. This lesion renders the motor slightly hypomorphic at
197 the permissive 15°C (with 91% of embryos remaining viable and fertile) but complete mitotic spindle
198 collapse occurs in as little as 30 seconds upon upshift, suggesting that DHC-1 motor function has been
199 nearly completely ablated (O'rourke, Bowerman et al. 2007).

200 We expected that combining the *dhc-1(ts)* allele with fluorescently tagged SYS-1 would allow us
201 to examine a more penetrant dynein knockdown. This allowed us to overcome both redundancy
202 between dynein accessory chains in SYS-1 trafficking as well as the previously described incomplete or
203 pleiotropic effects of dynein depletion (Fig. 2A). We compared the CEI of P_{sys-1}:VENUS::SYS-1 (hereafter
204 VENUS::SYS-1) to that of mCherry::γ-Tubulin (TEI). SYS-1 and γ-Tubulin are both recruited to
205 centrosomes at a much higher rate during mitosis than in interphase (Vora and Phillips 2015; Raynaud-
206 Messina and Merdes 2007). Because *dhc-1(ts)* limits the extent of γ-Tubulin recruitment (Fig. 2B-C),
207 evaluating SYS-1 CEI as a ratio to g-Tubulin TEI ensures that decreases to the SYS-1 CEI must be
208 disproportionately large to be numerically distinct.

209 Consistent with the published hypomorphic nature of the allele at the permissive temperature
210 (O'rourke, Bowerman et al 2007), *dhc-1(ts)* embryosexhibit a notable decrease in the SYS-1 CEI of
211 embryos kept at the permissive temperature (Fig. 2 B-D). Following 30-45 seconds of temperature
212 upshift, the hypomorphic SYS-1 localization is enhanced, with severely reduced SYS-1 centrosomal
213 enrichment (Fig. 2B-C). While there was a decrease in centrosome size, presumably due to roles for
214 dynein in centrosome maturation (Priyanga, Bhakta-Guha et al 2021), we accounted for this by assessing
215 proportional changes in SYS-1 CEI compared to changes in γ-Tubulin TEI. We observed a CEI/TEI

216 decrease, corresponding to decreased centrosomal SYS-1 accumulation, proportionally greater than the
217 reduction in γ-tubulin (Fig. 2D'). When compared to the individual dynein subunit knockdown, the more
218 penetrant phenotype of *dhc-1(ts)* mutants indicates that SYS-1 requires the dynein microtubule motor
219 complex to localize appropriately to centrosomes. Additionally, it seems likely that redundancy of
220 peripheral motor components or incomplete knockdown is indeed responsible for the variability within
221 individual subunit depletions seen above (Fig 1C-C').

222 **Microtubule Depolymerization Experiments Reveal that SYS-1 Centrosomal Dynamics are Affected**
223 **both Positively and Negatively by Microtubule-Mediated Trafficking**

224 To determine the extent to which microtubule-based trafficking in general is responsible for SYS-
225 1 centrosomal localization, we treated gravid adults and their embryos with >100 μM nocodazole, a
226 microtubule-destabilizing agent. This dose, while sufficient for a rapid acute response in adult animals,
227 resulted in either no effect on fertilized embryos because of the eggshell or prevented the production of
228 additional embryos via germline arrest (unpublished data). We therefore turned to a lower dose, longer-
229 term nocodazole treatment: 12 hours at 25μg/mL (83 μM). Maternal nocodazole treatment allowed us
230 to obtain embryos with limited microtubule networks, but sufficient spindle development to enter
231 mitosis (Fig. 3A). Surprisingly, the centrosomal enrichment of SYS-1::GFP driven by a general maternal
232 promoter (P_{pie-1}::GFP::SYS-1, hereafter GFP::SYS-1) increased after nocodazole treatment (Fig. 3B, C).

233 The observed SYS-1 CEI increase in nocodazole treated embryos is similar to the phenotype
234 observed in RPT-4 depletion, which decreases proteasome function (Vora and Phillips, 2015). To ensure
235 that this change in SYS-1 localization was not because of off-target effects, we compared maternal
236 feeding to that of *perm-1(RNAi)* permeabilized embryos. When treated with 10.5 μM nocodazole, these
237 embryos formed sufficient microtubule networks to enter mitosis and form spindles, but these spindles
238 were often inappropriately rotated or positioned (61% of imaged embryos, N=11/18), suggesting that

239 astral microtubules have been severely disrupted (Fig. S4A). We observed a similar CEI increase in
240 GFP::SYS-1 in these embryos (Fig. S4B). This could be consistent with a model where both SYS-1
241 recruitment to centrosomes and SYS-1 proteasomal degradation are affected by disruptions to
242 microtubule mediated trafficking. In this model subtle disruptions to dynein trafficking would limit the
243 ability of SYS-1 to replenish its mobile fraction, reducing SYS-1 centrosomal enrichment (Phillips and
244 Vora 2015). However, more severe disruptions to dynein function could be sufficient for defective
245 localization of the regulatory process, preventing clearance of SYS-1 and increasing its centrosomal
246 enrichment.

247 As different subsets of dynein and microtubule depletions exhibit either increased or decreased
248 SYS-1 CEI, we investigated a combination of these treatments to observe the behavior of SYS-1 upon
249 further disruption to microtubule-mediated trafficking. While both temperature upshift for *dhc-1(ts)* and
250 nocodazole treatments significantly affect SYS-1 centrosomal localization, neither treatment appears to
251 completely disrupt microtubule mediated trafficking. Nocodazole-treated embryos still exhibit some
252 kinetochore microtubules (Fig. 3A) but can tolerate weakly poisoned microtubules for some time.
253 Conversely, *dhc-1(ts)* embryos demonstrate severe loss of dynein function when reared at the restrictive
254 temperature. Thus short-term temperature upshifts are required to establish spindles and maintain
255 viability, suggesting that some portion of centrosomal trafficking during mitosis still occurs.”. We
256 therefore tested the combination of these treatments.

257 In contrast to embryos with GFP:SYS-1 driven by the strong early embryonic PIE-1 promoter (Fig.
258 3 B-C), embryos containing P_{sys-1}::VENUS::SYS-1, driven by the weaker endogenous SYS-1 promoter,
259 exhibit only a slight, non-significant, increase in CEI/TEI when treated with nocodazole (Fig. 3D, 1st and
260 2nd columns). However, when P_{sys-1}::VENUS::SYS-1 centrosomal enrichment is challenged by the
261 hypomorphic *dhc-1(ts)* at the permissive temperature, nocodazole treatment is sufficient to significantly

262 increase SYS-1 centrosomal recruitment. The finding that sensitizing embryos for dynein trafficking
263 defects is required to observe a nocodazole phenotype for P_{sys-1}::VENUS::SYS-1, but not for P_{pie-}
264 $_{1}$::GFP::SYS-1 indicates that the difference in transgene expression uncover a differential nocodazole
265 sensitivity in centrosomal recruitment of SYS-1. However, nocodazole-mediated increase in P_{pie-}
266 $_{1}$::GFP::SYS-1 centrosomal enrichment is no longer observed when the nocodazole treated *dhc-1(ts)*
267 embryos are upshifted to the restrictive temperature, suggesting that the increased SYS-1 centrosomal
268 enrichment seen in nocodazole treated embryos still requires dynein trafficking.

269 These observations describe a centrosomal relationship wherein treatments limiting the
270 coverage of microtubule-mediated dynein trafficking (i.e. nocodazole treatment) increase centrosomal
271 SYS-1 because of relatively inefficient or rare trafficking events for SYS-1 negative regulators, while
272 transient severe disruptions to dynein trafficking processivity (dynein subunit RNAi depletion, *dhc-1(ts)*
273 temperature upshift, upshift + nocodazole) reveal that SYS-1 centrosomal enrichment requires continual
274 replenishment via a functional microtubule motor.

275 If the nocodazole induced SYS-1 CEI increase described above is indeed due to a role for
276 microtubule-mediated trafficking in the centrosomal enrichment of some component of the SYS-1
277 degradation pathway, we would expect this proteolytic activity to be similarly mislocalized upon
278 trafficking disruption. Therefore, we decided to test the idea that proteasomal trafficking to, and
279 enrichment at, the centrosome was also perturbed in nocodazole-affected microtubule networks. We
280 first attempted to localize the proteasome. While the centrosome has been demonstrated to exhibit
281 proteolytic activity (Vora and Phillips 2015; Vora and Phillips 2016; Hames, Fry et al 2005; Peel,
282 O'Connell et al 2012; Wigley, Thomas et al 1999; Fabunmi, DeMartino et al 2000), existing
283 immunohistochemical reagents for mammalian proteasome subunits did not display any distinct
284 localization pattern in our embryos. An mCherry tag on proteasome subunit RPT-1 did demonstrate a

285 kinetochore microtubule enrichment, similar to that of DHC-1 and SYS-1, but appeared absent from
286 centrosomes. Inability to localize tagged RPT-1 may be due to a relatively low RPT-1 copy number per
287 proteasome, or correspondingly low proteasome number, limiting its relative enrichment. Alternatively,
288 fluorescently tagged proteins have shown evidence of degradation of the tag at a site of active
289 proteolysis, particularly if such a tag limits proteasome activity (Huang, Lobel et al 2014). To circumvent
290 this issue, we assayed for centrosomal proteasome activity indirectly by functionally testing an
291 additional centrosomal target of the RPT-4 containing proteasome, the centriole duplicating kinase ZYG-
292 1 (O'Connell, White et al 2001; Peel, O'Connell et al 2012). We additionally assayed therole of ECPS-1,
293 the *C. elegans* homolog of mammalian ECM29, which is an adaptor protein that enhances local
294 proteolytic activity of proteasomes via its function linking the dynein motor complex and the
295 proteasome and regulating 26S proteasome distribution (Gorbea, Rechsteiner et al 2004; Gorbea,
296 Rechsteiner et al 2010; Hsu, Cheng et al 2015; Ibañez-Vega, Yuseff et al 2021).

297 Knockdown of ECM29 homolog ECPS-1 (formerly D2045.2) resulted in embryos that displayed
298 an average 33.4% increase in centrosomal P_{pie-1}::GFP::SYS-1 enrichment, similar to both nocodazole-
299 treated and *rpt-4(RNAi)* embryos (Fig. 4A, Fig. 3A-C). Therefore, the overall increase in SYS-1 CEI seen in
300 nocodazole and *ecps-1(RNAi)* treated embryos suggests that microtubule mediated trafficking enhances
301 the removal of SYS-1 from centrosomes as well. Given the role of ECM29 in regulating the distribution
302 of proteasome complexes via microtubule-mediated trafficking, these data suggest that an improperly
303 localized proteasome in ecps-1(RNAi) results in dysregulation of SYS-1 similar to that seen in proteasome
304 functional knockdown (rpt-4(RNAi)) or broader depletion of microtubules (nocodazole treatment). To
305 determine if the effects of ECPS-1 knockdown are specific to SYS-1 dysregulation, or may be due to more
306 widespread effects on centrosomally localized proteins, we assayed an additional target. The ZYG-1
307 protein, a regulatory kinase controlling centriolar duplication, is both centrosomally enriched during
308 mitosis and negatively regulated by the RPT-4 proteasome (Peel, O'Connell et al 2012).. Utilizing a

309 fluorescently tagged ZYG-1 fragment demonstrated to mirror the localization and dynamics of the
310 endogenous protein (Peters, O'Connell et al 2010), we demonstrated 20% and 27% increased
311 accumulation of ZYG-1 in both proteasome knockdown *rpt-4(RNAi)* and *ecps-1(RNAi)* treatments,
312 respectively. The similarity of phenotype between nocodazole, ECPS-1 depletion, and RPT-4 proteasome
313 knockdown implies a functional link between microtubule-mediated trafficking of centrosomally
314 localized proteins and their eventual degradation by the RPT-4 proteasome.

315 Because SYS-1 centrosomal recruitment depends on rapid degradation via the centrosomal
316 proteasome (Vora and Phillips 2015), we assayed the mobile fraction of centrosomal SYS-1 in *ecps-*
317 *1(RNAi)* by FRAP. Comparison of GFP::SYS-1 recovery after photobleach demonstrated that depletion of
318 ECPS exhibits an intermediate phenotype between *rpt-4(RNAi)* proteasome depletion and negative
319 controls (Figure G-G"). While the initial rate of *ecps-1(RNAi)* GFP::SYS-1 recovery was similar to that seen
320 in wild type embryos, the late recovery phase of *ecps-1(RNAi)* embryos showed an early SYS-1 recovery
321 plateau, evidence of a significantly reduced mobile fraction that was intermediate to wild type and
322 proteasome depleted *rpt-4(RNAi)* embryos (Fig. 4E,G). The recovery curve observed in *ecps-1(RNAi)*
323 suggests that SYS-1 recovers at an approximately wild type rate in *ecps-1(RNAi)* embryos but remains
324 approximately as immobile as in proteasome-depleted embryos. Therefore, ECPS-1 depleted embryos
325 appear to degrade SYS-1 incompletely, as observed in the RPT-4 proteasome depletion, but with
326 sufficient protein turnover to enable wild type recruitment of newly trafficked SYS-1.

327 While both P_{pie-1}:SYS-1::GFP and P_{pie-1}::GFP::ZYG-1c exhibit an increase in their CEI as a result of
328 *ecps-1(RNAi)*, their turnover rates at the centrosome are not similarly affected. This may be due to
329 diverging regulatory pathways en route to the RPT-4 proteasome, or differences in the availability of
330 binding sites at the centrosome specific to each protein. Meanwhile, ECPS-1 depleted embryos may be
331 unaffected in protein clearance per proteasome, but the delayed or partial localization of the

332 centrosomal proteasome could result in hierarchical stabilization of a spatially or temporally inaccessible
333 fraction consisting of highly expressed and continually trafficked proteins, like SYS-1.

334 **Dynein Trafficking is Required for Restriction of Wnt-Signaled Cell Fates**

335 Having established a two-fold role for SYS-1 regulation in microtubule-mediated trafficking, we
336 investigated the role microtubule trafficking played in regulating SYS-1 dependent cell fate decisions.
337 Since the SYS-1 centrosomal localization pattern has been seen across all examined SYS-1-expressing
338 tissues (Phillips, Kimble et al 2007; Huang, Lin et al 2007; Baldwin and Phillips 2018; Lam and Phillips
339 2017), we investigated cell fate changes in embryonic and larval tissues across one embryonic and two
340 larval SYS-1 dependent cell fate decisions. These included a transcriptional reporter of the *end-1* WβA
341 target gene in the establishment of SYS-1 dependent endoderm, and anatomical markers for larval
342 specification of the stem cell-like hypodermal seam cells and the germline stem cell niche.

343 First, to directly assay the effect of centrosomal dysregulation of transcriptional activator SYS-1,
344 we investigated the nuclear enrichment of GFP::SYS-1 after division of the Wnt-regulated
345 endomesodermal precursor cell (EMS)(Bei, Mello et al 2002). In the EMS division, SYS-1 is enriched in
346 the posterior E nucleus, but not that of the anterior MS (Fig. 5A-B). Analyzing nuclear enrichment of
347 green fluorescence protein (GFP)-tagged SYS-1, we were able to observe increased nuclear GFP signal in
348 both the E and MS daughters in analyzed trafficking mutants (Fig. 5C). Interestingly, daughters affected
349 by both *ecps-1(RNAi)* and *dlc-1(RNAi)* exhibit significant enhancement of nuclear enrichment in each of
350 the two daughter cells (Fig 5C), suggesting that these treatments act negatively on SYS-1, despite
351 opposing effect on SYS-1 centrosomal enrichment. Following loss of negative centrosomal regulation,
352 these data suggest that daughter cell SYS-1 inheritance is increasing and thus affecting the bias of the
353 EMS asymmetric division, increasing the likelihood of unsignaled daughter cells adopting the signaled
354 endoderm cell fate.

355 Having established an increase in nuclear GFP::SYS-1 in dynein subunit depletion, even in cells
356 not signaled to stabilize SYS-1, we turned to the effect of SYS-1 expression on target gene activation.
357 Specifically, we used the endogenous promoter of WβA target gene *end-1* to drive GFP-tagged Histone
358 2B in order to evaluate the activity of SYS-1 immediate downstream targets as the signaled E cell
359 established the endoderm tissue expansion from 2 to 4 to 8 cells (E+1, +2, or +3 divisions, respectively).
360 Normally, this strain exhibits additional expression of the *end-1* promoter in <10% of embryos, a
361 frequency which decreases further when SYS-1 is depleted via RNAi (Fig. 5D). In embryos depleted of
362 either dynein subunits or RSA-2 by RNAi, however, we observed a different pattern. In these embryos,
363 misregulation via dynein depletion appeared to increasingly overwhelm SYS-1 negative regulation in
364 successive divisions, such that each generation after SYS-1 dependent specification increasingly
365 expresses the *end-1* promoter driven endodermal reporter outside of the EMS lineage (Fig. 5D). For
366 instance, in *dhc-1(RNAi)* we observe only 3% of embryos mis-expressing one cell division after the
367 specification of the E cell type (E+1), which increases to 25% by the next division (E+2), and over 83%
368 three divisions after specification (E+3).

369 We also investigated larval ACDs to determine the effect that extra transcriptionally active SYS-1
370 has on organismal development. We examined the seam cells (SCs) and distal tip cells (DTCs) because of
371 their sensitivity to SYS-1 dependent gene activation (Baldwin, Phillips et al 2016; Baldwin and Phillips
372 2018; Lam and Phillips 2017; Mila, Putzke et al 2015). In wild-type animals, DTC lineages undergo
373 asymmetric cell division during L1 to give rise to two DTCs, while *sys-1* mutants and animals
374 overexpressing SYS-1 show loss or gain of DTCs, respectively, due to symmetric cell division (Fig 6A)
375 (Miskowski, Kimble et al 2001; Siegfried, Kimble et al 2004; Kidd, Kimble et al 2005; Chesney, Kimble et
376 al 2009). To further sensitize these cells for changes in SYS-1 dependent cell fate changes, we examined
377 strains containing additional, transgenic SYS-1 driven by the heat shock promoter. In animals that are
378 not subjected to heat shock, dynein depletion only rarely induced development of more than the

379 endogenous 2 distal tip or 16 seam cells (Fig. 6B, 7B). In heat shocked animals, excess SYS-1 protein can
380 overwhelm canonical SYS-1 regulation to develop as many as 6 DTCs (Fig. 6D). While heat shock-induced
381 overexpression is sufficient to cause a notable shift towards the signaled cell fate, dynein subunit
382 depletion was able to significantly enhance the effect of heat shock (Fig. 6C). Depletion of DHC-1 or
383 ECPS-1 at the time of the somatic gonadal precursor division was sufficient to induce rare but wild-type-
384 unobserved additional DTCs (0.3% of animals for these 2 treatments, N= 394, 363, respectively). Adding
385 heat shock-overexpressed SYS-1 enhanced the penetrance of ectopic DTCs, with DHC-1 and ECPS-1
386 depletion resulting in populations where 11.9% and 6.8% of animals, respectively, develop more than 2
387 DTCs. Depletion of RSA-2, uncoupling SYS-1 from centrosomes, and depletion of the dynein light chain
388 DYLT-1 further enhanced these misspecifications, increasing the proportion of the population with
389 ectopic DTCs from 26.6% in wild type to 33.6% or 51% after RNAi depletion, respectively (Fig. 6D).

390 The SC lineage also undergoes several WβA-dependent ACDs throughout larval development
391 (Fig 7A, B). Similarly, in the SC tissue, depletion of dynein light chains alone is sufficient to increase the
392 frequency of ectopic SCs from 3.3% of larvae with ectopic SCs in control RNAi conditions to 11.7% or
393 10% of animals as seen in DYLT-1 and DLC-1 depletions, respectively (Fig. 7C). These misspecifications
394 are further exacerbated by SYS-1 overexpression, wherein more than 60% of the *dylt-1(RNAi)* larvae
395 have greater than wild type seam cell numbers, developing as many as 21 SCs, (Fig. 7D). These
396 observations collectively support SYS-1 centrosomal enrichment by dynein as a mechanism to reinforce
397 SYS-1 function in specifying SYS-1-dependent cell fate decisions. Therefore, compromising the
398 centrosomal SYS-1 regulatory system by dynein depletion is rarely sufficient to induce misspecifications
399 in otherwise wildtype animals, but notably enhances the effects of ectopic SYS-1 accumulation.
400 Therefore, dynein-dependent centrosomal regulation of transcriptional coactivator SYS-1 increases the
401 robustness of WβA-regulated cell fate decisions after ACD.

402 **Discussion**

403 Precise control of cell fate determinants is critical for normal development and homeostasis,
404 particularly in the rapidly dividing cells of the early embryo. Regulation of these factors includes the
405 distribution and inheritance of these determinants by daughter cells. Here we demonstrate that
406 centrosomal negative regulation of *C. elegans* β-catenin SYS-1 is enhanced during asymmetric division
407 by trafficking to centrosomes by the microtubule motor dynein. Depletion of individual dynein subunits
408 or associated proteins is sufficient to reduce the enrichment of centrosomal SYS-1, and temporally
409 specific ablation of dynein function by *dhc-1(ts)* was sufficient to remove observable SYS-1 nearly
410 completely and disproportionately from centrosomes. However, some methods of disrupting
411 dynein/microtubule trafficking result in an unexpected increase in centrosomal accumulation of SYS-1
412 protein. These increases, caused by microtubule disruption via nocodazole and depletion of SYS-1
413 negative regulator adapter ECPS-1, phenocopy the increased centrosomal enrichment and immobile
414 fraction of SYS-1 seen in *rpt-4(RNAi)* depletion. We therefore propose a model wherein both SYS-1 and
415 regulatory components of the ubiquitin-proteasome system, are dependent on microtubule-mediated
416 trafficking to centrosomes by the dynein complex in order to appropriately reinforce SYS-1 asymmetric
417 regulation across daughter cells (Fig. 8).

418 In this model, SYS-1 enriches at centrosomes and is degraded or marked for degradation before
419 leaving the centrosome. Rather than a static centrosomal enrichment, this model entails continual
420 trafficking by microtubule motors to maintain an observable centrosomal pool of SYS-1. The observable
421 CEI then measures a steady state of centrosomal enrichment at centrosomes, wherein SYS-1 is localized
422 to centrosomes more rapidly than it is marked and cleared. SYS-1 therefore becomes visibly enriched at
423 centrosomes compared to cytoplasmic levels. This model predicts that even subtle disruptions to
424 microtubule mediated trafficking could limit the ability of cells to maintain wild type SYS-1 centrosomal
425 enrichment, assuming the SYS-1 clearance rate remains unchanged.

426 Interestingly, the *rsa-2(RNAi)* enhancement of kinetochore localization of SYS-1 in this model is
427 consistent with 'traffic jams' observed in microtubule mediated trafficking (Leduc, Howard et al 2012). In
428 these cases, crowding motors by increasing the local concentration of motor proteins, introducing
429 microtubule-binding obstacles, or, importantly for our model, preventing terminal motor dissociation
430 limits the activity of motor proteins (Nam and Epureanu, 2017; Ferro, Yildiz et al 2019). Evidence of
431 traffic jams in vivo have been shown in neuronal microtubule transport, as neuronal kinesin and its
432 cargo synaptotagmin accumulate when trafficking is disrupted by hypomorphic kinesin alleles. The
433 disrupted motor complexes then accumulate upstream of the trafficking impediment, in an
434 accumulation of both motor and cargo (Hurd and Saxton 1996).

435 The kinetochore localization of SYS-1 is consistent with a traffic jam model, thus making SYS-1
436 trafficking by microtubule motors a more attractive model. Decreasing centrosomal SYS-1 localization by
437 *rsa-2(RNAi)* increases SYS-1 protein in resulting daughter cells (Vora and Phillips 2015). A severely
438 limited centrosomal recruitment of SYS-1 in *rsa-2(RNAi)* may also suggest problematic SYS-1/motor
439 protein unloading upon reaching the MTOC centrosome. Similarly, P_{pie-1}::GFP::SYS-1, which appears
440 overexpressed compared to P_{sys-1}::VENUS::SYS-1, may exacerbate SYS-1 traffic jams by increasing the
441 cytoplasmic SYS-1 pool. In either case, the combination of P_{pie-1}::GFP::SYS-1 and *rsa-2(RNAi)* results in a
442 further increase in the incidence of SYS-1 localization to kinetochore microtubules, suggesting increased
443 SYS-1 levels coupled with decreased centrosomal capturing may reveal an otherwise transient pool of
444 SYS-1 en route to the MTOC centrosome. Inefficient SYS-1 capture in *rsa-2(RNAi)* embryos likely further
445 crowds SYS-1-containing microtubule motor complexes into 'traffic jams' because, in embryos lacking a
446 mechanism to anchor SYS-1 to the centrosome, SYS-1 is trafficked toward centrosomes more quickly
447 than it is captured there and processed. This shift results in an observable SYS-1 accumulation at regions
448 of high microtubule occupancy, such as kinetochore microtubules and the cell cortex, both of which are
449 increased after RSA-2 depletion.

450 Conversely, centrosomal protein processing by either post-translational modifications or
451 degradation via the proteasome likely requires the trafficking of fewer, yet reusable enzymes. The
452 disparity between substrate vs enzyme trafficking requirements would suggest that clearance of
453 centrosomal substrates is less vulnerable to mild or short-term disruptions to trafficking than the
454 maintenance of a centrosomal substrate pool. Upon long-term or severe disruptions to microtubule
455 trafficking, a trafficking requirement for clearance mechanisms becomes apparent. Our model predicts
456 that disruption of either SYS-1 localization (inefficient trafficking to the site of regulation) or disrupting
457 the localization of a member of the Ubiquitin-Proteasome System (UPS) (where SYS-1 is trafficked and
458 accumulates, but centrosomal regulation/degradation is ineffective) both result in increased SYS-1
459 dependent gene activation and differentiation in daughter cells, consistent with excessive inheritance.
460 While this system of centrosomal localization and clearance of SYS-1 does not appear necessary for most
461 WβA differentiation events, disruptions to SYS-1 trafficking or processing limit the system's ability to
462 tolerate perturbations. That is, SYS-1 centrosomal localization generates robustness in SYS-1 dependent
463 cell fate decisions (Fig. -7) due to parallel trafficking mechanisms; disrupting either trafficking
464 mechanism results in excessive SYS-1 dependent activity in daughter cells of mothers with either
465 increased or decreased SYS-1 CEI.

466 Why does no single dynein disruption treatment fully recapitulate the *rsa-2(RNAi)* phenotype?
467 While we see individuals within several dynein knockdown treatments with nearly *rsa-2(RNAi)*-like SYS-1
468 centrosomal uncoupling, these populations also include embryos with roughly wild type centrosomal
469 SYS-1 enrichment. However, given the severely deleterious nature of dynein subunit loss-of-functions
470 (Sönnichsen, Neumann et al 2005) and the variability of feeding RNAi knockdowns as compared to null
471 mutant strains (Tavernarakis, Driscoll et al 2000), it seems likely that our significant decreases in SYS-1
472 centrosomal recruitment represent a phenotypically incomplete knockdown. Surviving embryos then
473 only exhibit hypomorphic dynein function, insufficient to induce catastrophic defects in spindle

474 assembly but sufficient to affect SYS-1 centrosomal enrichment. However, it is also possible that there is
475 partial redundancy between the SYS-1 relevant functions of the dynein motor. Introducing *dhc-1(ts)*
476 overcomes either incomplete knockdown or redundancy since a thorough dynein disruption can
477 robustly uncouple centrosomal SYS-1.

478 Why, then, do we observe an increase in centrosomal SYS-1 steady state upon either long term
479 lower dose nocodazole-mediated knockdowns of trafficking or by RNAi depletion of trafficking subunit
480 ECPS-1? In response to these data (Fig. 3), we propose the additional trafficking of a SYS-1 negative
481 regulatory component to this model. Disrupting the trafficking of centrosomal SYS-1 negative regulators
482 should result in a previously unseen increase in centrosomal SYS-1 steady state, while exhibiting a
483 similar effect on SYS-1 retention in daughter cells, downstream gene expression, and cell fate decisions
484 (Fig. 3-7). However, the difference in SYS-1 enrichment between most dynein depletions and that of
485 ECPS-1 or nocodazole treatment suggests a differential efficiency in trafficking or centrosomal capture
486 rate between SYS-1 and its negative regulators, such as the proteasome.

487 Most disruptions to the dynein motor that reduce SYS-1 centrosomal accumulation, mediated
488 by maternally fed RNAi, are consistent but likely incomplete because of their requirement for oogenesis
489 and early embryonic viability. Relatively mild dynein knockdowns resulting in viable embryos are likely
490 able to form dynein complexes, but at a far reduced rate. These dynein-limited embryos should
491 therefore decrease the rate of continual SYS-1 trafficking while not preventing the centrosomal
492 localization of an occasional regulatory components, perhaps of the Ubiquitin-Proteasome System
493 (UPS). The reusable tagging or proteolytic machinery is likely sufficient to enzymatically process SYS-1
494 that still localizes to the centrosome, but the rate of incoming SYS-1 is significantly reduced. Similarly,
495 depletion of dynein function by *dhc-1(ts)* effectively depletes all dynein function but can only do so for
496 brief portions of mitosis without inducing mitotic spindle collapse.

497 While dynein depletions limit the volume of trafficking by limiting the number of properly
498 constructed dynein motors, they do not limit the ability of an individual, functional dynein motor to
499 traffic. The experimental conditions that increase the steady state of centrosomal SYS-1, nocodazole and
500 *ecps-1(RNAi)*, instead limit the scope of dynein cargo trafficking. ECPS-1, putative adapter between
501 dynein and the proteasome, increases the steady state of both SYS-1 and additional centrosomal
502 proteasome target ZYG-1. Increased enrichment of both proteins is consistent with the conserved role
503 of ECM29 for ECPS-1, and results in embryos that are not inhibited for overall dynein function but
504 limited in their ability to traffic proteasome. Nocodazole treatment similarly does not directly affect the
505 processivity of dynein complexes that form on the comparatively limited microtubule network.
506 However, it does severely affect the reach of the microtubule network itself (Fig. 3A). Our data therefore
507 suggests that the proteasome requires less continual reinforcement by microtubule-mediated trafficking
508 but does require more extensive microtubule formation than is allowed in our nocodazole-treated
509 embryos.

510 A role for trafficking in both SYS-1 and its regulatory components, then, suggests a differentially
511 maintained steady state interaction for the proteasome and centrosomal SYS-1. While SYS-1 is rapidly
512 and continuously trafficked, it is also rapidly processed by centrosomal regulatory proteins. That is, the
513 apparently rapid processing of centrosomal SYS-1 also requires rapid dynein-mediated flux to maintain
514 its centrosomal steady state. Any disruption to dynein processivity will therefore allow slower SYS-1
515 centrosomal enrichment to be overcome by its centrosomal processing, reducing the SYS-1 CEI by
516 slowing the transfer of SYS-1 from cytoplasm to centrosome for degradation. By comparison, the
517 proteasome or ubiquitin ligases endure at the centrosome, continually processing centrosomal targets.
518 Our proposed model therefore predicts that short term or partial disruptions to the dynein motor (Fig.
519 8, red inset) allow for the eventual establishment of a centrosomal proteolysis pathway, which may
520 affect both SYS-1 and proteasome localization, but nevertheless result in decreasing steady state levels

521 of centrosomal SYS-1 (and presumably other proteasome targets that require active trafficking) as
522 occasional proteasome centrosomal localization overcomes the impaired localization of SYS-1.
523 Conversely, long term systemic disruptions to microtubule-mediated motors like that seen in
524 nocodazole treatment may still capture SYS-1 in their comparatively limited microtubule network, while
525 being disproportionately deprived of the larger proteasome complex (Fig. 8, blue inset).

526 Our model that both SYS-1 and its regulators are trafficked was supported but the identification
527 of a trafficking component that affects one but not both arms of our trafficking model. Most of our
528 perturbations, generally affecting components of the dynein machinery, may exert their effects by
529 either detaching SYS-1 from the motor or by sabotaging all function of the motor complex. However, the
530 specificity of our two transport mechanisms was exhibited by one dynein-protein interaction, via
531 depletion of ECPS-1/the putative ECM29 subunit of the motor. Unlike the other subunits presenting
532 strong SYS-1 phenotypes, ECM29 has not yet been implicated in dynein function beyond its adaptor role
533 but has notable effects on proteasome localization and response to stress (Gorbea, Rechsteiner et al
534 2010; Haratake, Chiba et al 2016). Because *ecps-1(RNAi)* phenocopies the centrosomal GFP::SYS-1
535 accumulation seen in proteasome knockdown via *rpt-4(RNAi)* as well as microtubule network disruption
536 via nocodazole treatment, we propose that these observations support a role for proteasomal
537 localization as well as function for proper centrosomal clearance of SYS-1 (Fig. 8).

538 While this model and our experiments to test it have been largely centered on SYS-1/β-catenin,
539 many developmental and temporally regulated proteins are known to pass through the centrosome
540 (Vora and Phillips 2016; Brown, Welch et al 1994; Johnston, Kopito et al 1998; Huang and Raff 1999;
541 Reck-Peterson, Carter et al 2018), as the centrosomal proteasome is far from SYS-1-specific. It is not
542 unreasonable, then, to presume that other proteins may benefit from dynein trafficking to something as
543 short-lived and yet influential to daughter cell inheritance as the mitotic centrosome. Particularly early
544 in eukaryotic development, subtle changes in the inheritance of cell fate determinants like SYS-1 can

545 have a profound effect on the ability of an organism to respond to environmental insults. For example,
546 the asymmetric nuclear localization of SYS-1 indicative of differential cell fate has been shown to arise
547 early, less than 70 seconds after the establishing division (Baldwin and Phillips 2014; Vora and Phillips
548 2015). We therefore propose that an active dynein mediated trafficking, at least for cell fate
549 determinants like SYS-1, could provide a universal buffering against excessive inheritance and
550 consequentially rare but deleterious cell fate changes.

551 **Materials and Methods**

552 **Strains**

553 Strains were maintained on Op50-inoculated Nematode Growth Media (NGM) plates at 15°
554 (BTP51, BTP220) or 25° C (TX964, BTP51, LP563, TX691) using typical *C. elegans* methods. These strains
555 contained the following transgenes and alleles: **N2** (wild type); **TX964** (unc-119(ed3) III; him-3(e1147) IV;
556 teis98 [P_{pie-1}::GFP::SYS-1]); **BTP51** (unc-119(ed3) III; tjIs71 [pie-1 promoter::mCherry::H2B, pie-1
557 promoter::2x mCherry::tbg-1, unc-119(+)]; qIs95 III) ; **BTP220** (unc-119(ed3) III; tjIs71 [pie-1
558 promoter::mCherry::H2B, pie-1 promoter::2x mCherry::tbg-1, unc-119(+)]; qIs95 III; dhc-1(or195) I.) ;
559 **TX691** (unc-119(ed3) III; teIs46 [pRL1417; end-1p::GFP::H2B + unc-119(+)]) ; **OC341 (**unc-119(ed3) III;
560 bsIs8[pMS5.1:unc -119(+) pie -1- gfp-zyg-1C-terminus]); **BTP93** (*wIs78[SCMp::GFP + ajm-1p::GFP +*
561 *F58E10* (cosmid) *+ unc-119(+*)] *IV; uiwEx22*[*pHS::sys-1*]); **BTP97** (*qIs56[lag-2p::GFP + unc-119(+)]*
562 *V;uiwIs3[pHS::sys-1*]); **AZ235** (*unc-119(ed3) III; ruIs48[Ppie-1::gfp::tbb-1*]); **TH107 (**P_{pie-1}::RSA-2:: GFP)

563 **RNAi**

564 To perform RNAi knockdown of target genes, we used HT115 bacteria containing the pL4440
565 plasmid with a T7-flanked target gene insert. Most of these were obtained from a library supplied by the
566 Ahringer lab via Addgene (Kamath and Ahringer 2003). Those which were otherwise obtained (dlc-1)
567 used target gene-flanking primers with *C. elegans* cDNA to generate a new insert. These bacteria were

568 used to seed Isopropyl β- d-1-thiogalactopyranoside (IPTG)-containing, inducing plates as described
569 previously. Worms were generally plated to RNAi after Sodium Hypochlorite Synchronization as L1's.
570 More deleterious knockdowns (*dlc-1, dhc-1)* were washed from OP50 plates at 24 hours before imaging
571 (L3/L4) or 12 hours before imaging (late L4/early adult) (Timmons 2006; Bekas and Phillips 2020). DLC-1
572 was derived using RT primers and digested with Xho I and HIND III.

573 **Compound Microscopy, CEI, and Image Processing**

574 To obtain samples, mothers were anesthetized with 250 μM levamisole and dissected *via* a
575 clean surgical blade. Embryos were then transferred to a 2% agarose pad and imaged on a Zeiss Axio
576 Imager.D2. All exposure times were kept constant. Centrosomal measurements were collected from the
577 mitotic P1 cell of the early embryo during anaphase, at approximately similar inter-polar distance (Fig.
578 S5). Images were exported as uncompressed TIF's, and fluorescence intensity was determined by
579 measuring the mean fluorescence of centrosomal puncta in ImageJ. The mean intensity of the remaining
580 embryonic cytoplasm was subtracted from the centrosomal mean to produce the CEI measurement, and
581 identical measurements on 2x mCherry::tbg-1 were used for TEI. END-1 family nuclei were assayed via
582 the TX691 strain. GFP-tagged Histone intensity was measured relative to the cytoplasmic
583 autofluorescence.

584 **Temperature Sensitive Allele Imaging**

585 BTP51 and BTP220 were maintained together at 15°C and were imaged as above. Ambient
586 temperature in the microscope room was decreased to ~18°C for 'permissive' imaging and upshifted to
587 'restrictive' 26°C by moving slides to a Pecon Tempcontroller 2000-2 heated stage. Embryos were
588 imaged at the two temperatures sequentially, with approx. 45 seconds between upshift and image, or
589 were imaged as populations at either the permissive or restrictive temperature.

590 **Nocodazole Treatment**

591 In order to treat embryos before formation of the drug-impermeable eggshell, we exposed late
592 L4's to a low dose (approx. 83 μM, 25 μg/mL) nocodazole dissolved in 2% dimethyl sulfoxide (DMSO) for
593 16 hours. Embryos were then concentrated by one minute centrifugation at 1000xG and imaged as
594 described above. Permeabilization of embryos was performed as described in Carvalho, Oegema et al
595 2011. Imaging was done as described above, but included 4% sucrose and 0.1M NaCl to the 2% agar
596 pads to bolster embryo stability (Greenan, Hyman et al 2010; Gönczy, Schnabel et al 1999).

597 **Confocal Microscopy and Fluorescence Recovery After Photobleach**

598 Confocal microscopy was performed via a Leica SP8 HyD detector system. The objective used
599 was a 63x HC PL APO CS2 objective with N.A. = 1.4, utilizing type F immersion oil. Each image analyzed
600 consisted of the sum of 35 z-images across the embryo, each slice approximately 0.35 μm thick. FRAP
601 was performed on the same system. Each embryo was imaged twice before bleaching, beginning as
602 soon as possible after Nuclear Envelope BreakDown (NEBD). The ROI, an approximately 5μm square,
603 was then bleached at an intermediate focal plane with 100% laser power for 100 iterations. Images were
604 taken as above, once every 7 seconds. Fluorescence intensity was measured on summed slice Z-
605 projections in FIJI via the mean fluorescence intensity of ROIs drawn around relevant locales – either
606 centrosome or the entire dividing cell. Recovery was assayed by subtracting the ROI post-bleach
607 intensity from each measurement and evaluating it as a percentage of the pre-bleached centrosomal
608 intensity.

609 **Heat Shock-Induced SYS-1 Overexpression**

610 BTP93 and BTP97 worms were exposed to brief 33℃ heat shocks at relevant developmental
611 timepoints to drive SYS-1 overexpression concurrently with signaled cell fate specification. For DTCs,
612 BTP97 was subjected to 1-hour heat shock, 30-minutes recovery, and 30-minutes additional heat shock
613 beginning 11.5 hours after plating. For SCs, BTP93 was subjected to 2-hour heat shock, 30-minute

614 recovery, and additional 1-hour heat shock beginning 26 hours after plating. Both tissue types were
615 assayed 50 hours after plating.

616 **Acknowledgements**

617 We thank Kimberly Bekas and Amy Clemons for helpful comments on the manuscript. Strains
618 were provided by the Caenorhabditis Genetics Center, which is funded by the National Institutes of
619 Health (NIH) Office of Research Infrastructure Programs [P40 OD01440], or gifts from the laboratory of
620 Tony Hyman (TH107) and Kevin F. O'Connell at the NIDDK (OC341). This work was supported by NIH
621 award NIH GM114007 (B.T.P.).

622

623

624

625

626

627

628 **References**

629 Amsterdam, A., F. Pitzer and W. Baumeister (1993). "Changes in intracellular localization of proteasomes
630 in immortalized ovarian granulosa cells during mitosis associated with a role in cell cycle control." Proc
631 Natl Acad Sci U S A **90**(1): 99-103.
632 Baldin, V., M. Militello, Y. Thomas, C. Doucet, W. Fic, S. Boireau, I. Jariel-Encontre, M. Piechaczyk, E.
633 Bertrand, J. Tazi and O. Coux (2008). "A novel role for PA28gamma-proteasome in nuclear speckle
634 organization and SR protein trafficking." Mol Biol Cell **19**(4): 1706-1716.

635 Baldwin, A. T., A. M. Clemons and B. T. Phillips (2016). "Unique and redundant beta-catenin regulatory
636 roles of two Dishevelled paralogs during C. elegans asymmetric cell division." J Cell Sci **129**(5): 983-993.
637 Baldwin, A. T. and B. T. Phillips (2014). "The tumor suppressor APC differentially regulates multiple beta-
638 catenins through the function of axin and CKIalpha during C. elegans asymmetric stem cell divisions." J
639 Cell Sci **127**(Pt 12): 2771-2781.
640 Baldwin, A. T. and B. T. Phillips (2018). Chapter 3 - Cell Polarity and Asymmetric Cell Division by the Wnt
641 Morphogen. Cell Polarity in Development and Disease. P. Michael Conn. Boston, Academic Press**:** 61-
642 102.
643 Bei, Y., J. Hogan, L. A. Berkowitz, M. Soto, C. E. Rocheleau, K. M. Pang, J. Collins and C. C. Mello (2002).
644 "SRC-1 and Wnt signaling act together to specify endoderm and to control cleavage orientation in early
645 C. elegans embryos." Dev Cell **3**(1): 113-125.
646 Bekas, K. N. and B. T. Phillips (2020). "Generating reliable hypomorphic phenocopies by RNAi using long
647 dsRNA as diluent." MicroPubl Biol **2020**.
648 Ben-Yaakov, K., S. Y. Dagan, Y. Segal-Ruder, O. Shalem, D. Vuppalanchi, D. E. Willis, D. Yudin, I. Rishal, F.
649 Rother, M. Bader, A. Blesch, Y. Pilpel, J. L. Twiss and M. Fainzilber (2012). "Axonal transcription factors
650 signal retrogradely in lesioned peripheral nerve." EMBO J **31**(6): 1350-1363.
651 Brown, C. R., S. J. Doxsey, E. White and W. J. Welch (1994). "Both viral (adenovirus E1B) and cellular (hsp
652 70, p53) components interact with centrosomes." J Cell Physiol **160**(1): 47-60.
653 Bullock, S. L. and D. Ish-Horowicz (2001). "Conserved signals and machinery for RNA transport in
654 Drosophila oogenesis and embryogenesis." Nature **414**(6864): 611-616.
655 Carminati, J. L. and T. Stearns (1997). "Microtubules orient the mitotic spindle in yeast through dynein-
656 dependent interactions with the cell cortex." J Cell Biol **138**(3): 629-641.
657 Carvalho, A., S. K. Olson, E. Gutierrez, K. Zhang, L. B. Noble, E. Zanin, A. Desai, A. Groisman and K.
658 Oegema (2011). "Acute drug treatment in the early C. elegans embryo." PLoS One **6**(9): e24656.

659 Chesney, M. A., N. Lam, D. E. Morgan, B. T. Phillips and J. Kimble (2009). "C. elegans HLH-
660 2/E/Daughterless controls key regulatory cells during gonadogenesis." Dev Biol **331**(1): 14-25.
661 Deshimaru, M., M. Kinoshita-Kawada, K. Kubota, T. Watanabe, Y. Tanaka, S. Hirano, F. Ishidate, M.
662 Hiramoto, M. Ishikawa, Y. Uehara, H. Okano, S. Hirose, S. Fujioka, K. Iwasaki, J. Yuasa-Kawada, T.
663 Mishima and Y. Tsuboi (2021). "DCTN1 Binds to TDP-43 and Regulates TDP-43 Aggregation." Int J Mol Sci
664 **22**(8).
665 Fabunmi, R., W. Wigley, P. Thomas and G. DeMartino (2000). "Activity and Regulation of the
666 Centrosome-associated Proteasome." Journal of Biological Chemistry **275**: 409-413.
667 Ferenz, N. P., A. Gable and P. Wadsworth (2010). "Mitotic functions of kinesin-5." Seminars in cell &
668 developmental biology **21**(3): 255-259.
669 Ferro, L. S., S. Can, M. A. Turner, M. M. ElShenawy and A. Yildiz (2019). "Kinesin and dynein use distinct
670 mechanisms to bypass obstacles." Elife **8**.
671 Fuchs, E. and T. Chen (2013). "A matter of life and death: self-renewal in stem cells." EMBO Rep **14**(1):
672 39-48.
673 Gao, F. J., L. Shi, T. Hines, S. Hebbar, K. L. Neufeld and D. S. Smith (2017). "Insulin signaling regulates a
674 functional interaction between adenomatous polyposis coli and cytoplasmic dynein." Mol Biol Cell **28**(5):
675 587-599.
676 Geyer, F. C., M. Lacroix-Triki, K. Savage, M. Arnedos, M. B. Lambros, A. MacKay, R. Natrajan and J. S.
677 Reis-Filho (2011). "beta-Catenin pathway activation in breast cancer is associated with triple-negative
678 phenotype but not with CTNNB1 mutation." Mod Pathol **24**(2): 209-231.
679 Gómez-López, S., R. G. Lerner and C. Petritsch (2014). "Asymmetric cell division of stem and progenitor
680 cells during homeostasis and cancer." Cell Mol Life Sci **71**(4): 575-597.

681 Gönczy, P., H. Schnabel, T. Kaletta, A. D. Amores, T. Hyman and R. Schnabel (1999). "Dissection of Cell
682 Division Processes in the One Cell Stage Caenorhabditis elegans Embryo by Mutational Analysis." Journal
683 of Cell Biology **144**(5): 927-946.
684 Gorbea, C., G. M. Goellner, K. Teter, R. K. Holmes and M. Rechsteiner (2004). "Characterization of
685 mammalian Ecm29, a 26 S proteasome-associated protein that localizes to the nucleus and membrane
686 vesicles." J Biol Chem **279**(52): 54849-54861.
687 Gorbea, C., G. Pratt, V. Ustrell, R. Bell, S. Sahasrabudhe, R. E. Hughes and M. Rechsteiner (2010). "A
688 protein interaction network for Ecm29 links the 26 S proteasome to molecular motors and endosomal
689 components." J Biol Chem **285**(41): 31616-31633.
690 Hames, R. S., R. E. Crookes, K. R. Straatman, A. Merdes, M. J. Hayes, A. J. Faragher and A. M. Fry (2005).
691 "Dynamic recruitment of Nek2 kinase to the centrosome involves microtubules, PCM-1, and localized
692 proteasomal degradation." Mol Biol Cell **16**(4): 1711-1724.
693 Hanz, S., E. Perlson, D. Willis, J. Q. Zheng, R. Massarwa, J. J. Huerta, M. Koltzenburg, M. Kohler, J. van-
694 Minnen, J. L. Twiss and M. Fainzilber (2003). "Axoplasmic importins enable retrograde injury signaling in
695 lesioned nerve." Neuron **40**(6): 1095-1104.
696 Harada, A., Y. Takei, Y. Kanai, Y. Tanaka, S. Nonaka and N. Hirokawa (1998). "Golgi vesiculation and
697 lysosome dispersion in cells lacking cytoplasmic dynein." J Cell Biol **141**(1): 51-59.
698 Haratake, K., A. Sato, F. Tsuruta and T. Chiba (2016). "KIAA0368-deficiency affects disassembly of 26S
699 proteasome under oxidative stress condition." J Biochem **159**(6): 609-618.
700 He, T. C., A. B. Sparks, C. Rago, H. Hermeking, L. Zawel, L. T. da Costa, P. J. Morin, B. Vogelstein and K. W.
701 Kinzler (1998). "Identification of c-MYC as a target of the APC pathway." Science **281**(5382): 1509-1512.
702 Horgan, C. P., S. R. Hanscom, R. S. Jolly, C. E. Futter and M. W. McCaffrey (2010). "Rab11-FIP3 links the
703 Rab11 GTPase and cytoplasmic dynein to mediate transport to the endosomal-recycling compartment."
704 J Cell Sci **123**(Pt 2): 181-191.

705 Hsu, M. T., C. L. Guo, A. Y. Liou, T. Y. Chang, M. C. Ng, B. I. Florea, H. S. Overkleeft, Y. L. Wu, J. C. Liao and
706 P. L. Cheng (2015). "Stage-Dependent Axon Transport of Proteasomes Contributes to Axon
707 Development." Dev Cell **35**(4): 418-431.
708 Huang, J. and J. W. Raff (1999). "The disappearance of cyclin B at the end of mitosis is regulated spatially
709 in Drosophila cells." Embo j **18**(8): 2184-2195.
710 Huang, L., D. Pike, D. E. Sleat, V. Nanda and P. Lobel (2014). "Potential pitfalls and solutions for use of
711 fluorescent fusion proteins to study the lysosome." PLoS One **9**(2): e88893.
712 Huang, S., P. Shetty, S. M. Robertson and R. Lin (2007). "Binary cell fate specification during C. elegans
713 embryogenesis driven by reiterated reciprocal asymmetry of TCF POP-1 and its coactivator beta-catenin
714 SYS-1." Development **134**(14): 2685-2695.
715 Hurd, D. D. and W. M. Saxton (1996). "Kinesin mutations cause motor neuron disease phenotypes by
716 disrupting fast axonal transport in Drosophila." Genetics **144**(3): 1075-1085.
717 Ibañez-Vega, J., F. Del Valle, J. J. Sáez, F. Guzman, J. Diaz, A. Soza and M. I. Yuseff (2021). "Ecm29-
718 Dependent Proteasome Localization Regulates Cytoskeleton Remodeling at the Immune Synapse." Front
719 Cell Dev Biol **9**: 650817.
720 Jha, R. and T. Surrey (2015). "Regulation of processive motion and microtubule localization of
721 cytoplasmic dynein." Biochem Soc Trans **43**(1): 48-57.
722 Johnston, J. A., C. L. Ward and R. R. Kopito (1998). "Aggresomes: a cellular response to misfolded
723 proteins." J Cell Biol **143**(7): 1883-1898.
724 Juanes, M. A. (2020). "Cytoskeletal Control and Wnt Signaling-APC's Dual Contributions in Stem Cell
725 Division and Colorectal Cancer." Cancers (Basel) **12**(12).
726 Kamath, R. S., A. G. Fraser, Y. Dong, G. Poulin, R. Durbin, M. Gotta, A. Kanapin, N. Le Bot, S. Moreno, M.
727 Sohrmann, D. P. Welchman, P. Zipperlen and J. Ahringer (2003). "Systematic functional analysis of the
728 Caenorhabditis elegans genome using RNAi." Nature **421**(6920): 231-237.

729 Kidd, A. R., 3rd, J. A. Miskowski, K. R. Siegfried, H. Sawa and J. Kimble (2005). "A beta-catenin identified
730 by functional rather than sequence criteria and its role in Wnt/MAPK signaling." Cell **121**(5): 761-772.
731 Lam, A. K. and B. T. Phillips (2017). "Wnt Signaling Polarizes C. elegans Asymmetric Cell Divisions During
732 Development." Results Probl Cell Differ **61**: 83-114.
733 Leduc, C., K. Padberg-Gehle, V. Varga, D. Helbing, S. Diez and J. Howard (2012). "Molecular crowding
734 creates traffic jams of kinesin motors on microtubules." Proceedings of the National Academy of
735 Sciences **109**(16): 6100-6105.
736 Liu, W., X. Dong, M. Mai, R. S. Seelan, K. Taniguchi, K. K. Krishnadath, K. C. Halling, J. M. Cunningham, L.
737 A. Boardman, C. Qian, E. Christensen, S. S. Schmidt, P. C. Roche, D. I. Smith and S. N. Thibodeau (2000).
738 "Mutations in AXIN2 cause colorectal cancer with defective mismatch repair by activating beta-
739 catenin/TCF signalling." Nat Genet **26**(2): 146-147.
740 Loh, K. M., R. van Amerongen and R. Nusse (2016). "Generating Cellular Diversity and Spatial Form: Wnt
741 Signaling and the Evolution of Multicellular Animals." Dev Cell **38**(6): 643-655.
742 Mbom, B. C., K. A. Siemers, M. A. Ostrowski, W. J. Nelson and A. I. Barth (2014). "Nek2 phosphorylates
743 and stabilizes beta-catenin at mitotic centrosomes downstream of Plk1." Mol Biol Cell **25**(7): 977-991.
744 Mikenberg, I., D. Widera, A. Kaus, B. Kaltschmidt and C. Kaltschmidt (2007). "Transcription factor NF-
745 kappaB is transported to the nucleus via cytoplasmic dynein/dynactin motor complex in hippocampal
746 neurons." PLoS One **2**(7): e589.
747 Mila, D., A. Calderon, A. T. Baldwin, K. M. Moore, M. Watson, B. T. Phillips and A. P. Putzke (2015).
748 "Asymmetric Wnt Pathway Signaling Facilitates Stem Cell-Like Divisions via the Nonreceptor Tyrosine
749 Kinase FRK-1 in Caenorhabditis elegans." Genetics **201**(3): 1047-1060.
750 Miskowski, J., Y. Li and J. Kimble (2001). "The sys-1 gene and sexual dimorphism during gonadogenesis in
751 Caenorhabditis elegans." Dev Biol **230**(1): 61-73.

752 Mizumoto, K. and H. Sawa (2007). "Cortical beta-catenin and APC regulate asymmetric nuclear beta-
753 catenin localization during asymmetric cell division in C. elegans." Dev Cell **12**(2): 287-299.
754 Nam, W. and B. I. Epureanu (2017). "Dynamic model for kinesin-mediated long-range transport and its
755 local traffic jam caused by tau proteins." Phys Rev E **95**(1-1): 012405.
756 Niehrs, C. and S. P. Acebron (2012). "Mitotic and mitogenic Wnt signalling." EMBO J **31**(12): 2705-2713.
757 Niehrs, C. and S. P. Acebron (2012). "Mitotic and mitogenic Wnt signalling." EMBO J **31**(12): 2705-2713.
758 Nusse, R. and H. Clevers (2017). "Wnt/beta-Catenin Signaling, Disease, and Emerging Therapeutic
759 Modalities." Cell **169**(6): 985-999.
760 O'Connell, K. F., C. Caron, K. R. Kopish, D. D. Hurd, K. J. Kemphues, Y. Li and J. G. White (2001). "The C.
761 elegans zyg-1 gene encodes a regulator of centrosome duplication with distinct maternal and paternal
762 roles in the embryo." Cell **105**(4): 547-558.
763 O'Rourke, S. M., M. D. Dorfman, J. C. Carter and B. Bowerman (2007). "Dynein modifiers in C. elegans:
764 light chains suppress conditional heavy chain mutants." PLoS Genet **3**(8): e128.
765 Peel, N., M. Dougherty, J. Goeres, Y. Liu and K. F. O'Connell (2012). "The C. elegans F-box proteins LIN-23
766 and SEL-10 antagonize centrosome duplication by regulating ZYG-1 levels." J Cell Sci **125**(Pt 15): 3535-
767 3544.
768 Peters, N., D. E. Perez, M. H. Song, Y. Liu, T. Muller-Reichert, C. Caron, K. J. Kemphues and K. F. O'Connell
769 (2010). "Control of mitotic and meiotic centriole duplication by the Plk4-related kinase ZYG-1." J Cell Sci
770 **123**(Pt 5): 795-805.
771 Phillips, B. T., A. R. Kidd, 3rd, R. King, J. Hardin and J. Kimble (2007). "Reciprocal asymmetry of SYS-
772 1/beta-catenin and POP-1/TCF controls asymmetric divisions in Caenorhabditis elegans." Proc Natl Acad
773 Sci U S A **104**(9): 3231-3236.
774 Pintard, L. and B. Bowerman (2019). "Mitotic Cell Division in Caenorhabditis elegans." Genetics **211**(1):
775 35-73.

776 Pinto, D., A. Gregorieff, H. Begthel and H. Clevers (2003). "Canonical Wnt signals are essential for
777 homeostasis of the intestinal epithelium." Genes Dev **17**(14): 1709-1713.
778 Priyanga, J., G. Guha and D. Bhakta-Guha (2021). "Microtubule motors in centrosome homeostasis: A
779 target for cancer therapy?" Biochim Biophys Acta Rev Cancer **1875**(2): 188524.
780 Raynaud-Messina, B. and A. Merdes (2007). "Gamma-tubulin complexes and microtubule organization."
781 Curr Opin Cell Biol **19**(1): 24-30.
782 Reck-Peterson, S. L., W. B. Redwine, R. D. Vale and A. P. Carter (2018). "The cytoplasmic dynein
783 transport machinery and its many cargoes." Nat Rev Mol Cell Biol **19**(6): 382-398.
784 Reilein, A., D. Melamed, K. S. Park, A. Berg, E. Cimetta, N. Tandon, G. Vunjak-Novakovic, S. Finkelstein
785 and D. Kalderon (2017). "Alternative direct stem cell derivatives defined by stem cell location and
786 graded Wnt signalling." Nat Cell Biol **19**(5): 433-444.
787 Reya, T. and H. Clevers (2005). "Wnt signalling in stem cells and cancer." Nature **434**(7035): 843-850.
788 Sawa, H. (2012). "Control of cell polarity and asymmetric division in C. elegans." Curr Top Dev Biol **101**:
789 55-76.
790 Schlaitz, A. L., M. Srayko, A. Dammermann, S. Quintin, N. Wielsch, I. MacLeod, Q. de Robillard, A. Zinke,
791 J. R. Yates, 3rd, T. Müller-Reichert, A. Shevchenko, K. Oegema and A. A. Hyman (2007). "The C. elegans
792 RSA complex localizes protein phosphatase 2A to centrosomes and regulates mitotic spindle assembly."
793 Cell **128**(1): 115-127.
794 Schmidt, R., L. E. Fielmich, I. Grigoriev, E. A. Katrukha, A. Akhmanova and S. van den Heuvel (2017). "Two
795 populations of cytoplasmic dynein contribute to spindle positioning in C. elegans embryos." J Cell Biol
796 **216**(9): 2777-2793.
797 Shtutman, M., J. Zhurinsky, I. Simcha, C. Albanese, M. D'Amico, R. Pestell and A. Ben-Ze'ev (1999). "The
798 cyclin D1 gene is a target of the beta-catenin/LEF-1 pathway." Proc Natl Acad Sci U S A **96**(10): 5522-
799 5527.

800 Siegfried, K. R., A. R. Kidd, M. A. Chesney and J. Kimble (2004). "The sys-1 and sys-
801 3 Genes Cooperate With Wnt Signaling to Establish the Proximal-Distal Axis of the
802 Caenorhabditis elegans Gonad." Genetics **166**(1): 171-186.
803 Sonnichsen, B., L. B. Koski, A. Walsh, P. Marschall, B. Neumann, M. Brehm, A. M. Alleaume, J. Artelt, P.
804 Bettencourt, E. Cassin, M. Hewitson, C. Holz, M. Khan, S. Lazik, C. Martin, B. Nitzsche, M. Ruer, J.
805 Stamford, M. Winzi, R. Heinkel, M. Roder, J. Finell, H. Hantsch, S. J. Jones, M. Jones, F. Piano, K. C.
806 Gunsalus, K. Oegema, P. Gonczy, A. Coulson, A. A. Hyman and C. J. Echeverri (2005). "Full-genome RNAi
807 profiling of early embryogenesis in Caenorhabditis elegans." Nature **434**(7032): 462-469.
808 Sugioka, K., K. Mizumoto and H. Sawa (2011). "Wnt regulates spindle asymmetry to generate
809 asymmetric nuclear beta-catenin in C. elegans." Cell **146**(6): 942-954.
810 Sunchu, B. and C. Cabernard (2020). "Principles and mechanisms of asymmetric cell division."
811 Development **147**(13).
812 Tame, M. A., J. A. Raaijmakers, B. van den Broek, A. Lindqvist, K. Jalink and R. H. Medema (2014). "Astral
813 microtubules control redistribution of dynein at the cell cortex to facilitate spindle positioning." Cell
814 Cycle **13**(7): 1162-1170.
815 Tavernarakis, N., S. L. Wang, M. Dorovkov, A. Ryazanov and M. Driscoll (2000). "Heritable and inducible
816 genetic interference by double-stranded RNA encoded by transgenes." Nat Genet **24**(2): 180-183.
817 Tejpar, S., F. Nollet, C. Li, J. S. Wunder, G. Michils, P. dal Cin, E. Van Cutsem, B. Bapat, F. van Roy, J. J.
818 Cassiman and B. A. Alman (1999). "Predominance of beta-catenin mutations and beta-catenin
819 dysregulation in sporadic aggressive fibromatosis (desmoid tumor)." Oncogene **18**(47): 6615-6620.
820 Tetsu, O. and F. McCormick (1999). "Beta-catenin regulates expression of cyclin D1 in colon carcinoma
821 cells." Nature **398**(6726): 422-426.
822 Timmons, L. (2006). "Delivery methods for RNA interference in C. elegans." Methods Mol Biol **351**: 119-
823 125.

824 Vora, S. and B. T. Phillips (2015). "Centrosome-Associated Degradation Limits beta-Catenin Inheritance
825 by Daughter Cells after Asymmetric Division." Curr Biol **25**(8): 1005-1016.
826 Vora, S. M., J. S. Fassler and B. T. Phillips (2020). "Centrosomes are required for proper beta-catenin
827 processing and Wnt response." Mol Biol Cell **31**(17): 1951-1961.
828 Vora, S. M. and B. T. Phillips (2016). "The benefits of local depletion: The centrosome as a scaffold for
829 ubiquitin-proteasome-mediated degradation." Cell Cycle **15**(16): 2124-2134.
830 Wigley, W. C., R. P. Fabunmi, M. G. Lee, C. R. Marino, S. Muallem, G. N. DeMartino and P. J. Thomas
831 (1999). "Dynamic association of proteasomal machinery with the centrosome." J Cell Biol **145**(3): 481-
832 490.
833 Wójcik, C. and G. N. DeMartino (2003). "Intracellular localization of proteasomes." The International
834 Journal of Biochemistry & Cell Biology **35**(5): 579-589.
835 Wozniak, M. J., B. Bola, K. Brownhill, Y. C. Yang, V. Levakova and V. J. Allan (2009). "Role of kinesin-1 and
836 cytoplasmic dynein in endoplasmic reticulum movement in VERO cells." J Cell Sci **122**(Pt 12): 1979-1989.
837 Wühr, M., E. S. Tan, S. K. Parker, H. W. Detrich, 3rd and T. J. Mitchison (2010). "A model for cleavage
838 plane determination in early amphibian and fish embryos." Curr Biol **20**(22): 2040-2045.
839 Wühr, M., E. S. Tan, S. K. Parker, H. W. Detrich, 3rd and T. J. Mitchison (2010). "A model for cleavage
840 plane determination in early amphibian and fish embryos." Curr Biol **20**(22): 2040-2045.
841 Yang, L., X. Wu, Y. Wang, K. Zhang, J. Wu, Y. C. Yuan, X. Deng, L. Chen, C. C. Kim, S. Lau, G. Somlo and Y.
842 Yen (2011). "FZD7 has a critical role in cell proliferation in triple negative breast cancer." Oncogene
843 **30**(43): 4437-4446.
844 Zhunussova, G., G. Afonin, S. Abdikerim, A. Jumanov, A. Perfilyeva, D. Kaidarova and L. Djansugurova
845 (2019). "Mutation Spectrum of Cancer-Associated Genes in Patients With Early Onset of Colorectal
846 Cancer." Front Oncol **9**: 673.

847

848

849

850

851

852

853

854

855 **FIGURE LEGENDS**

856 **Figure 1:**

857 **Rationale and methodology for microtubule motor RNAi Screen.** A) GFP::SYS-1 can be occasionally
858 observed at regions corresponding to DHC-1 mitotic accumulation. This is particularly enhanced in
859 centrosomally uncoupled *rsa-2(RNAi)* embryos. The frequency of GFP::SYS-1 enrichment at these locales
860 in lacZ*(RNAi)* and rsa-2*(RNAi)* treatment is distinguished by color. A') GFP::SYS-1 at kinetochore
861 microtubule (white arrowhead) and cortex(black arrowhead) of the dividing *C. elegans* early embryo. B)
862 Demonstration of CEI and TEI calculation. CEI was calculated in FIJI by subtracting the mean pixel
863 intensity of a cytoplasmic ROI encompassing the proximal half of the dividing cell, approximated by the
864 light blue square, from a circular centrosome ROI, approximated by the white square. B') Expanded view
865 of ROI's as defined in B. B'') Graphical representation of the raw centrosomal and CEI adjusted
866 fluorescence intensity for the control (Left) and Affected (right) embryos in B. Control (*lacZ(RNAi)*
867 treated) exhibits both a high raw centrosomal GFP::SYS-1 and CEI. Affected (*rsa-2(RNAi)* treated) exhibits

868 an intermediate raw GFP::SYS-1, but severely decreased CEI, better reflecting its visual failure to
869 increase centrosomal GFP::SYS-1 notably above the bulk of cytoplasmic representation. C) Example
870 VENUS::SYS-1 CEI (C) and CEI/TEI (C') of controls and indicated dynein light chain depletions. Width of
871 the violin plot corresponds to a histogram of observation density. The median is indicated by the central
872 white dot, with the interquartile range indicated by the thick black line, and 1.5x additional Interquartile
873 range indicated by the thin black line. N= lacZ*(RNAi)*, 72; *dlc-1(RNAi),* 74; *dylt-1(RNAi),* 52; *rsa-2(RNAi)*,
874 22 * - p<0.05, *** - p<0.001 by Chi-square test (A) or Student's t-test (C-C').

875 **Figure 2:**

876 **The dynein heavy chain Temperature Sensitive (dhc-1(ts)) Allele mediated loss of dynein function has**
877 **a disproportionate effect on SYS-1 localization**. A) Diagram of the Dynein motor, and hypothetical
878 model of its role in SYS-1 trafficking. Relative location of *dhc-1(ts)* lesion indicated. B) Representative
879 centrosome images of VENUS::SYS-1 and g-Tubulin::mCherry in wildtype and ts allele-containing
880 embryos C) embryos at comparable cell cycle phase before (top) and after (bottom) temperature
881 upshift. D) SYS-1 CEI and D') SYS-1 CEI per TEI in embryos containing *dhc-1(ts)* , to control for differences
882 in centrosome assembly, standard error depicted. N= 44, 31, 38, 25 in D and D' columns, left to right. * -
883 p<0.05, ** - p<0.01, *** - p<0.001 by Student's t-test.

884 **Figure 3:**

885 **Nocodazole mediated disruption of microtubules enhances centrosomal GFP::SYS-1 enrichment** A)
886 Representative images of GFP::TBB-1 in DMSO and nocodazole treated embryos. White arrowheads
887 indicate astral microtubules (left) and the corresponding lack or dysregulated region in nocodazole
888 treatment (right) B) Quantification of, and C) Representative images of similarly treated GFP::SYS-1
889 embryos. For B, N=36 DMSO and 46 nocodazole treated embryos. * - p<0.05, ** - p<0.01 by Student's t-

890 test. D) CEI/TEI as evaluated with combinatorial Wildtype (WT) or *dhc-1(ts)* allele for Dynein Heavy
891 Chain, and treatment with 2% DMSO vehicle media or 2% DMSO + nocodazole media. Measurements at
892 the permissive and restrictive temperature are differentiated by blue and red coloring, respectively.
893 Error bars are SEM. E) Representative P_{sys-1}VENUS::SYS-1 and mCh::g-Tubulin for each treatment in D,
894 respectively.

895 **Figure 4:**

896 **Microtubule-mediated processes can also stabilize centrosomal SYS-1**. A) Treatment with *ecps-1(RNAi)*
897 enhances centrosomal SYS-1 accumulation, N=48 *lacZ(RNAi), N* =12 *rsa-2(RNAi), N*= 124 *ecps-1(RNAi).* B)
898 *lacZ(RNAi)* and *ecps-1(RNAi)* representative centrosomes in grayscale and intensity dependent look up
899 table (LUT). C) Putative dynein and proteasome adaptor ECPS-1 also appears to also enhance
900 centrosomal ZYG-1 accumulation, by GFP::ZYG-1c CEI (N=31 untreated, N=19 *ecps-1(RNAi),* N= 20 *rpt-*
901 *4(RNAi),* 14 *rsa-2(RNAi)*) and D) Representative GFP::ZYG-1c centrosomal images in grayscale and
902 intensity dependent LUT. (E-F) Quantified recovery of GFP::SYS-1 (E) and GFP::ZYG-1c (F) . Values
903 indicated are the ratio of bleached centrosomes to their prebleach value, normalized such that the
904 postbleach value, t = 0, is 0 GFP::SYS-1 intensity. Error bars are SEM. (G–G'') Representative FRAP
905 montage of 2nd division P1 cells in the indicated embryos. Two prebleach, immediately consecutive
906 time points are followed by the 1st postbleach image at time 0 and images every 7 s thereafter indicated
907 at the top left. *$p < 0.05$, **$p < 0.01$, ***$p < 0.001$ by Student's t test. One-sided Student's t test,
908 asterisk indicates p value from lacZ(RNAi) in E and F..

909 **Figure 5:**

910 **Effect of Dynein Depletion on nuclear SYS-1 Localization and Gene Expression in EMS Descendant**
911 **Cells**. A) The EMS precursor (embryo ventral cell) divides, receiving Wnt and Src specification and

912 orientation cues, respectively (red arrow). These daughters give rise to posterior, signaled E and
913 anterior, unsignaled MS daughter cells. Wildtype specification results in depicted approximate GFP::SYS-
914 1 localization pattern specifically enriched in the signaled daughter nucleus. B) Representative images of
915 wildtype and *ecps-1(RNAi)* treated embryos. Orange box encloses the unsignaled MS nucleus, Blue box
916 encloses the signaled E nucleus. C) Quantification of GFP::SYS-1 nuclear enrichment in indicated dynein
917 RNAi knockdowns. C') Mean difference in nuclear GFP::SYS-1 enrichment from quantification in C. Error
918 bars are SEM. D) Embryos ectopically expressing pEND-1::GFP::H2B in cells not descended from the E
919 lineage in the first (orange) second (blue) and third (green) lineage after the founding of the lineage (the
920 2, 4, and 8 cell E descendants, respectively). D') Representative embryos exhibiting WT (all lacZ*(RNAi)*-
921 treated, left) and ectopic (*ecps-1(RNAi)*- and 2x*dhc-1(RNAi)*- treated for 1, 2, and 3 generations after E
922 founding, respectively, right) P_{end-1}::GFP::H2B. *** - p<0.05, ** - p<0.01, *** - p<0.001**

923 **Figure 6:**

924 **SYS-1 dysregulation via dynein knockdown can cause rare distal tip cell fate conversions**. A) Diagram of
925 *C. elegans* distal tip cell signaled lineage specification in the somatic gonadal precursor. B)
926 Representative image of WT (top) and ectopically induced (bottom) distal tip cells (DTCs). To distinguish
927 DTC's from pLAG-2 driven vulval expression, DTCs are marked with white arrowheads. C) Number and
928 relative frequency of DTCs via anatomical marker in untreated animals and in backgrounds with RNAi
929 depletion of various dynein subunits. D) Number and relative frequency of DTCs marked by anatomical
930 marker when SYS-1 is overexpressed via a heat shock-driven transgene in both untreated animals and in
931 backgrounds with RNAi depletion of various dynein subunits. * = p<0.05, ** = p<0.01, *** = p<0.001 by
932 one-sided Mann-Whitney test

933 **Figure 7:**

934 **SYS-1 dysregulation via dynein knockdown can cause rare seam cell fate conversions.** A) Diagram of *C.*
935 *elegans* seam cell (SC) signaled lineage. B) Representative image of WT (top) and ectopically induced
936 (bottom) SCs. Likely ectopic SC exhibit spatially distinct 'doublets', highlighted here in brackets. C)
937 Number and relative frequency of SCs via anatomical marker when in untreated adults and in
938 backgrounds with RNAi depletion of various dynein subunits. D) Number and relative frequency of SCs
939 via anatomical marker when SYS-1 is overexpressed via a heat shock-driven transgene in both untreated
940 larvae and in backgrounds with RNAi depletion of various dynein subunits. * = $p<0.05$, ** = $p<0.01$, *** =
941 $p<0.001$ by Mann-Whitney test

942 **Figure 8:**

943 **Proposed model**. Speculation into the various processes by which SYS-1 and its regulators appear to be
944 localized to mitotic centrosomes. Both SYS-1 and some component of its centrosomal proteasome-
945 dependent negative regulators, here represented by purple circle, demonstrate some dependence on
946 microtubule mediated trafficking. While various dynein subunits are requisite components of a
947 functional dynein complex, the negative effect of their depletion on SYS-1 centrosomal steady state
948 indicates a preferential or more frequent trafficking of SYS-1. Relatively rare proteasome trafficking
949 events mediated by ECPS-1 meanwhile, are sufficient to maintain appropriate SYS-1 centrosomal
950 enrichment. This less efficient proteasomal trafficking, however, renders it vulnerable to nocodazole-
951 mediated decrease in overall microtubule trafficking/network formation efficiency. Red inset depicts
952 decreased processivity or cargo binding capacity induced by dynein light chain RNAi depletions. Blue
953 inset depicts depletion of adapter ECPS-1 and resulting depletion of proteasome-trafficking specific
954 dynein complexes, while not otherwise affecting the microtubule motor.

955

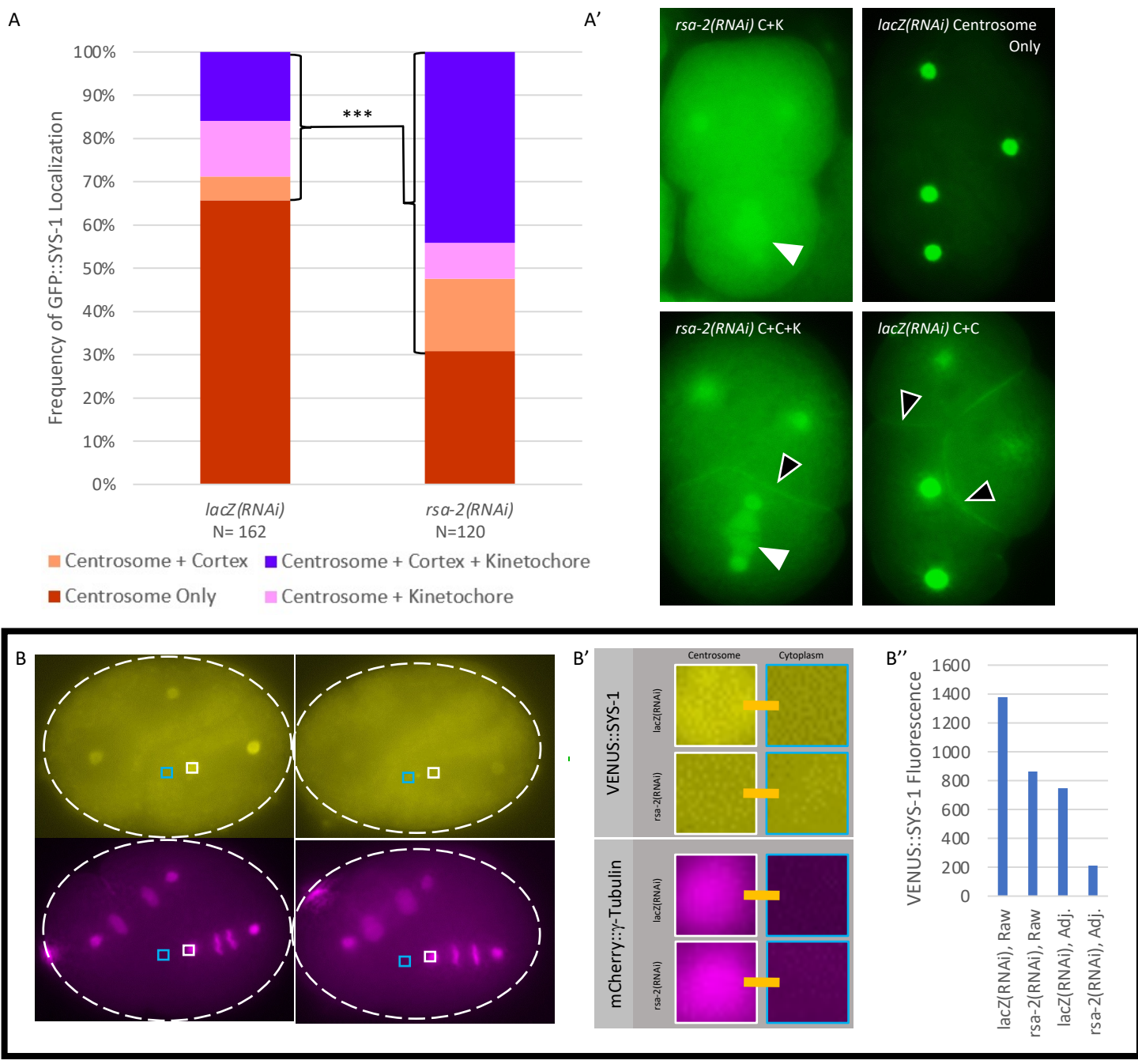
A
A'
Frequency of GFP::SYS-1 Localization
100%
90%
80%
70%
60%
50%
40%
30%
20%
10%
0%
***
lacZ(RNAi)
N= 162
rsa-2(RNAi)
N=120
Centrosome + Cortex
Centrosome + Cortex + Kinetochore
Centrosome Only
Centrosome + Kinetochore
rsa-2(RNAi) C+K
lacZ(RNAi) Centrosome Only
rsa-2(RNAi) C+C+K
lacZ(RNAi) C+C
B
B'
B''
VENUS::SYS-1
mCherry::γ-Tubulin
Centrosome
Cytoplasm
lacZ(RNAi)
rsa-2(RNAi)
VENUS::SYS-1 Fluorescence
1600
1400
1200
1000
800
600
400
200
0
lacZ(RNAi), Raw
rsa-2(RNAi), Raw
lacZ(RNAi), Adj.
rsa-2(RNAi), Adj.

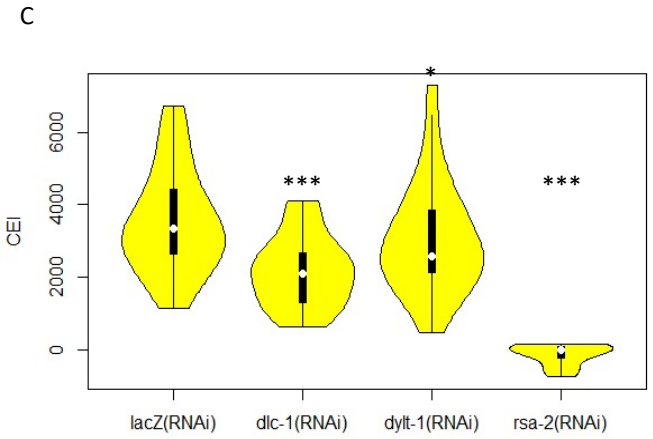
C
CEI
0
2000
4000
6000
*
***
***
lacZ(RNAi)
dlc-1(RNAi)
dylt-1(RNAi)
rsa-2(RNAi)

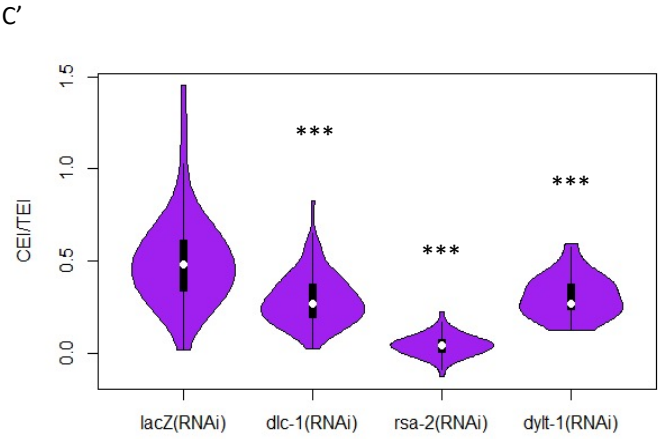
C'
CEI/TEI
0.0
0.5
1.0
1.5
***
***
***
lacZ(RNAi)
dlc-1(RNAi)
rsa-2(RNAi)
dylt-1(RNAi)

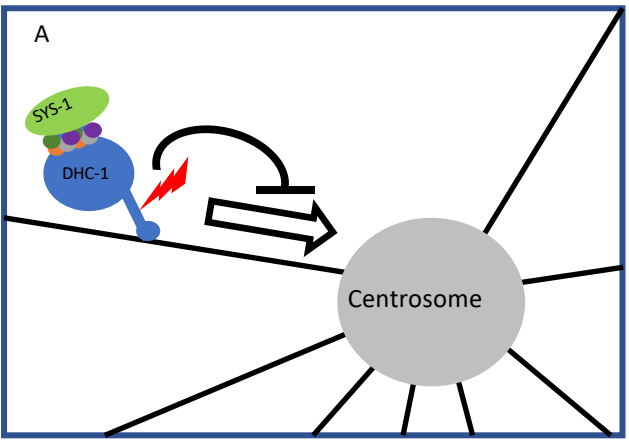
A
SYS-1
DHC-1
Centrosome

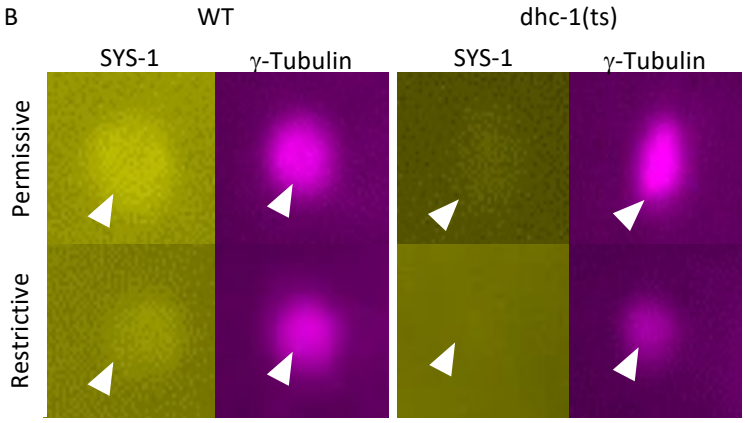
B
WT
dhc-1(ts)
SYS-1
γ-Tubulin
SYS-1
γ-Tubulin
Permissive
Restrictive

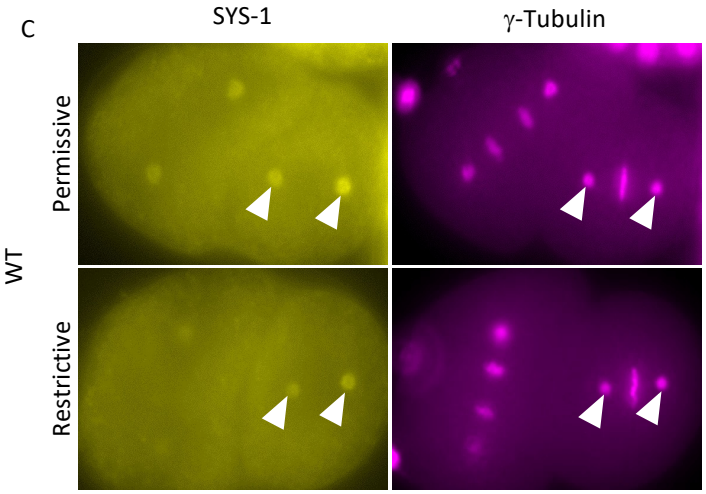
C
SYS-1
γ-Tubulin
WT
Permissive
Restrictive

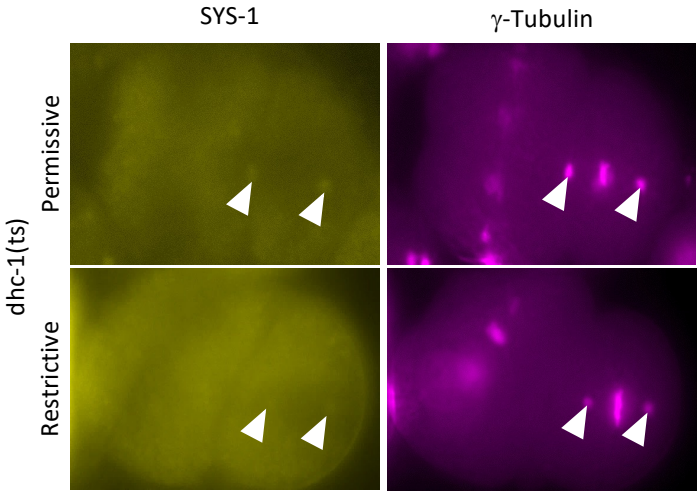
SYS-1
γ-Tubulin
dhc-1(ts)
Permissive
Restrictive

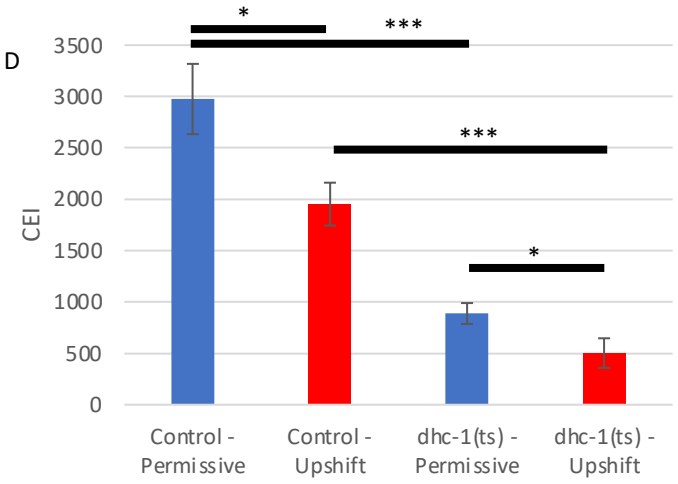
D
CEI
3500
3000
2500
2000
1500
1000
500
0
*
***
***
*
Control - Permissive
Control - Upshift
dhc-1(ts) - Permissive
dhc-1(ts) - Upshift

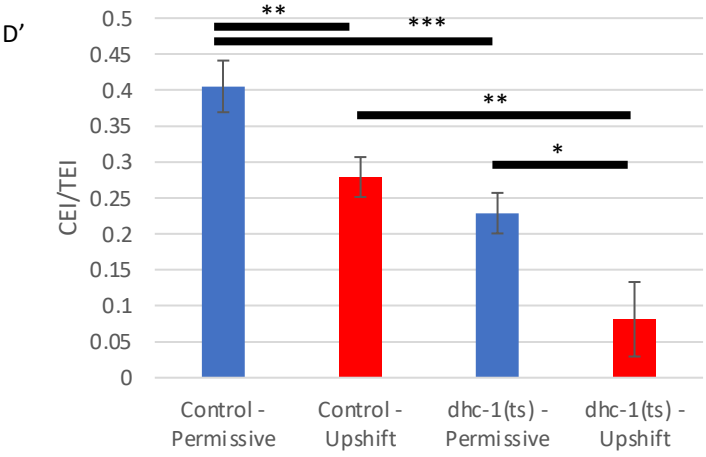
D'
CEI/TEI
0.5
0.45
0.4
0.35
0.3
0.25
0.2
0.15
0.1
0.05
0
**
***
**
*
Control - Permissive
Control - Upshift
dhc-1(ts) - Permissive
dhc-1(ts) - Upshift

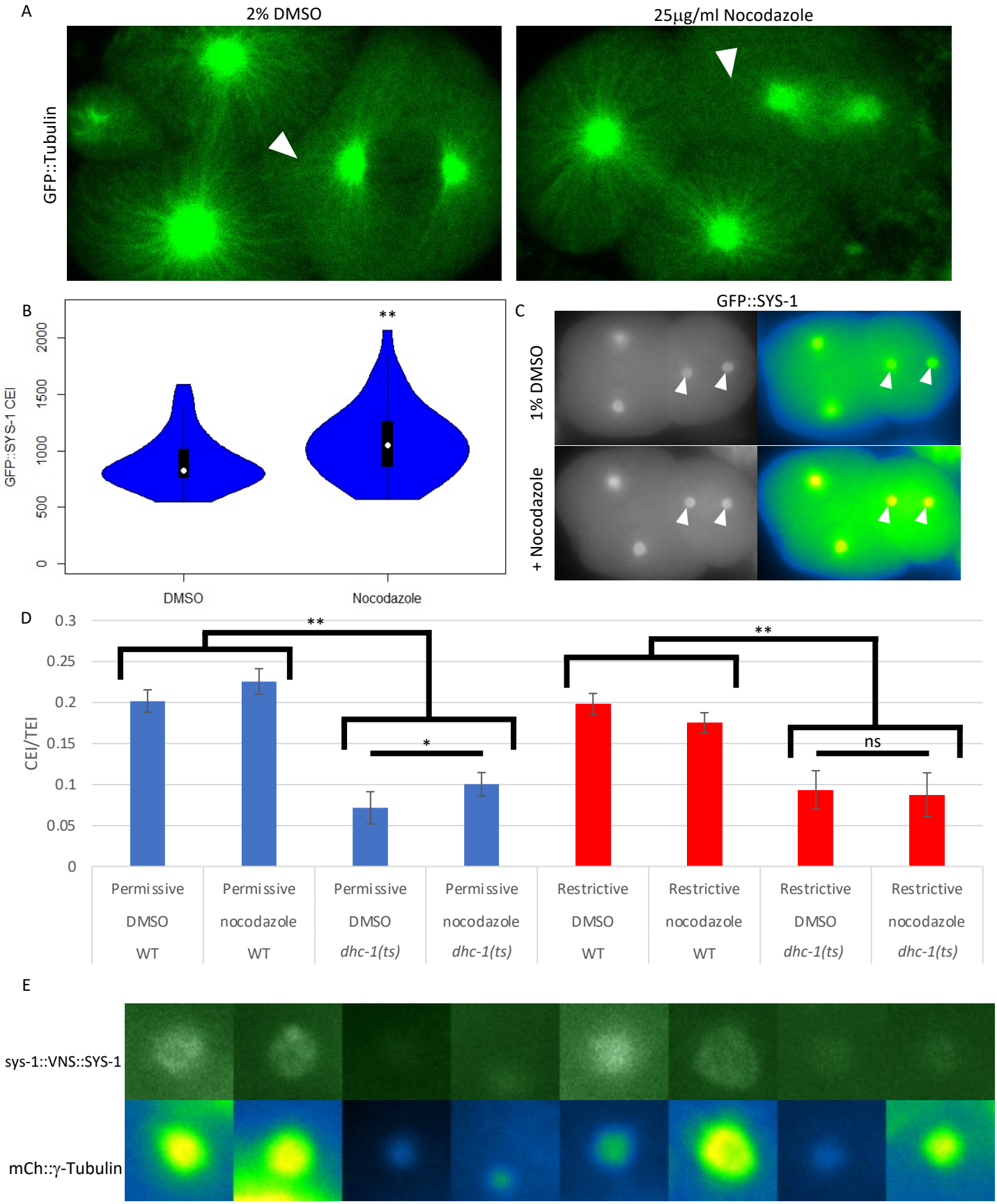
A
2% DMSO
25µg/ml Nocodazole
GFP::Tubulin
B
GFP::SYS-1 CEI
0
500
1000
1500
2000
**
DMSO
Nocodazole
C
GFP::SYS-1
1% DMSO
+ Nocodazole
D
CEI/TEI
0
0.05
0.1
0.15
0.2
0.25
0.3
**
*
**
ns
Permissive DMSO WT
Permissive nocodazole WT
Permissive DMSO dhc-1(ts)
Permissive nocodazole dhc-1(ts)
Restrictive DMSO WT
Restrictive nocodazole WT
Restrictive DMSO dhc-1(ts)
Restrictive nocodazole dhc-1(ts)
E
sys-1::VNS::SYS-1
mCh::γ-Tubulin

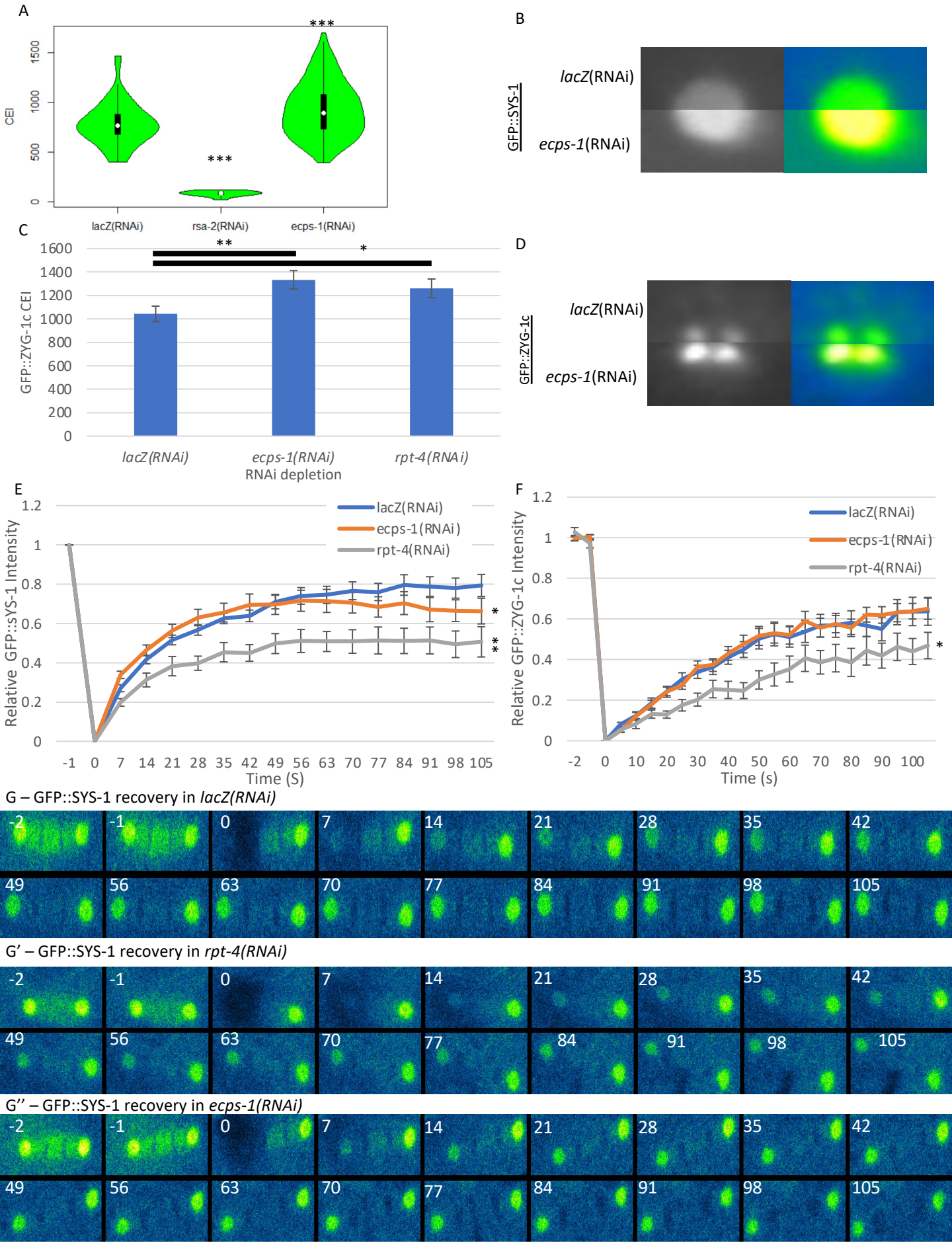
A
CEI
0
500
1000
1500
***
***
lacZ(RNAi)
rsa-2(RNAi)
ecps-1(RNAi)
B
GFP::SYS-1
lacZ(RNAi)
ecps-1(RNAi)
C
GFP::ZYG-1c CEI
0
200
400
600
800
1000
1200
1400
1600
**
*
lacZ(RNAi)
ecps-1(RNAi)
rpt-4(RNAi)
RNAi depletion
D
GFP::ZYG-1c
lacZ(RNAi)
ecps-1(RNAi)
E
Relative GFP::SYS-1 Intensity
0
0.2
0.4
0.6
0.8
1
1.2
lacZ(RNAi)
ecps-1(RNAi)
rpt-4(RNAi)
*
**
-1 0 7 14 21 28 35 42 49 56 63 70 77 84 91 98 105
Time (S)
F
Relative GFP::ZYG-1c Intensity
0
0.2
0.4
0.6
0.8
1
1.2
lacZ(RNAi)
ecps-1(RNAi)
rpt-4(RNAi)
*
-2 0 10 20 30 40 50 60 70 80 90 100
Time (s)
G – GFP::SYS-1 recovery in lacZ(RNAi)
-2 -1 0 7 14 21 28 35 42
49 56 63 70 77 84 91 98 105
G' – GFP::SYS-1 recovery in rpt-4(RNAi)
-2 -1 0 7 14 21 28 35 42
49 56 63 70 77 84 91 98 105
G'' – GFP::SYS-1 recovery in ecps-1(RNAi)
-2 -1 0 7 14 21 28 35 42
49 56 63 70 77 84 91 98 105

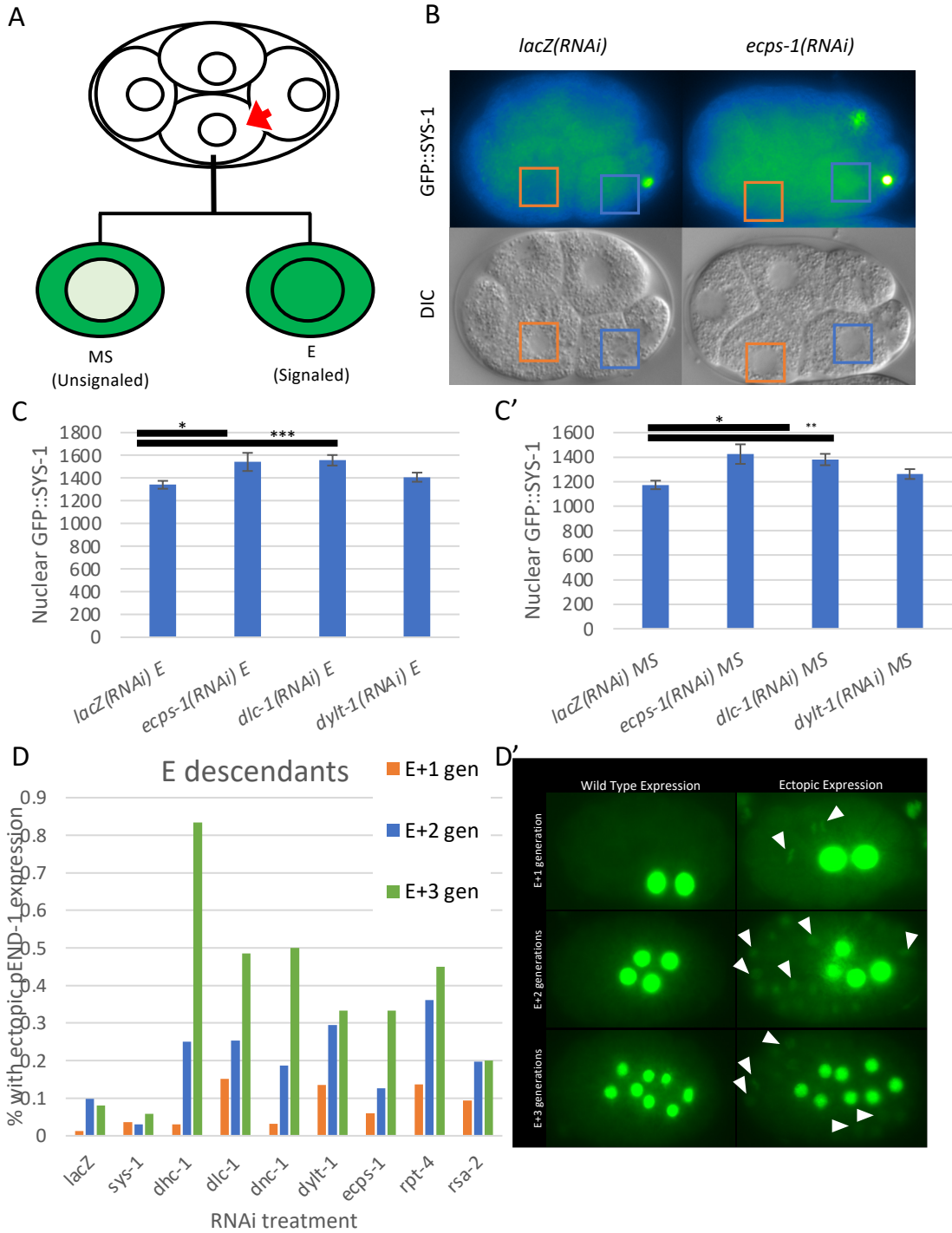
A
MS
(Unsignaled)
E
(Signaled)
B
lacZ(RNAi)
ecps-1(RNAi)
GFP::SYS-1
DIC
C
Nuclear GFP::SYS-1
1800
1600
1400
1200
1000
800
600
400
200
0
*
***
lacZ(RNAi) E
ecps-1(RNAi) E
dlc-1(RNAi) E
dylt-1(RNAi) E
C'
Nuclear GFP::SYS-1
1600
1400
1200
1000
800
600
400
200
0
*
**
lacZ(RNAi) MS
ecps-1(RNAi) MS
dlc-1(RNAi) MS
dylt-1(RNAi) MS
D
E descendants
E+1 gen
E+2 gen
E+3 gen
% with ectopic END-1 expression
0.9
0.8
0.7
0.6
0.5
0.4
0.3
0.2
0.1
0
lacZ
sys-1
dhc-1
dlc-1
dnc-1
dylt-1
ecps-1
rpt-4
rsa-2
RNAi treatment
D'
Wild Type Expression
Ectopic Expression
E+1 generation
E+2 generations
E+3 generations

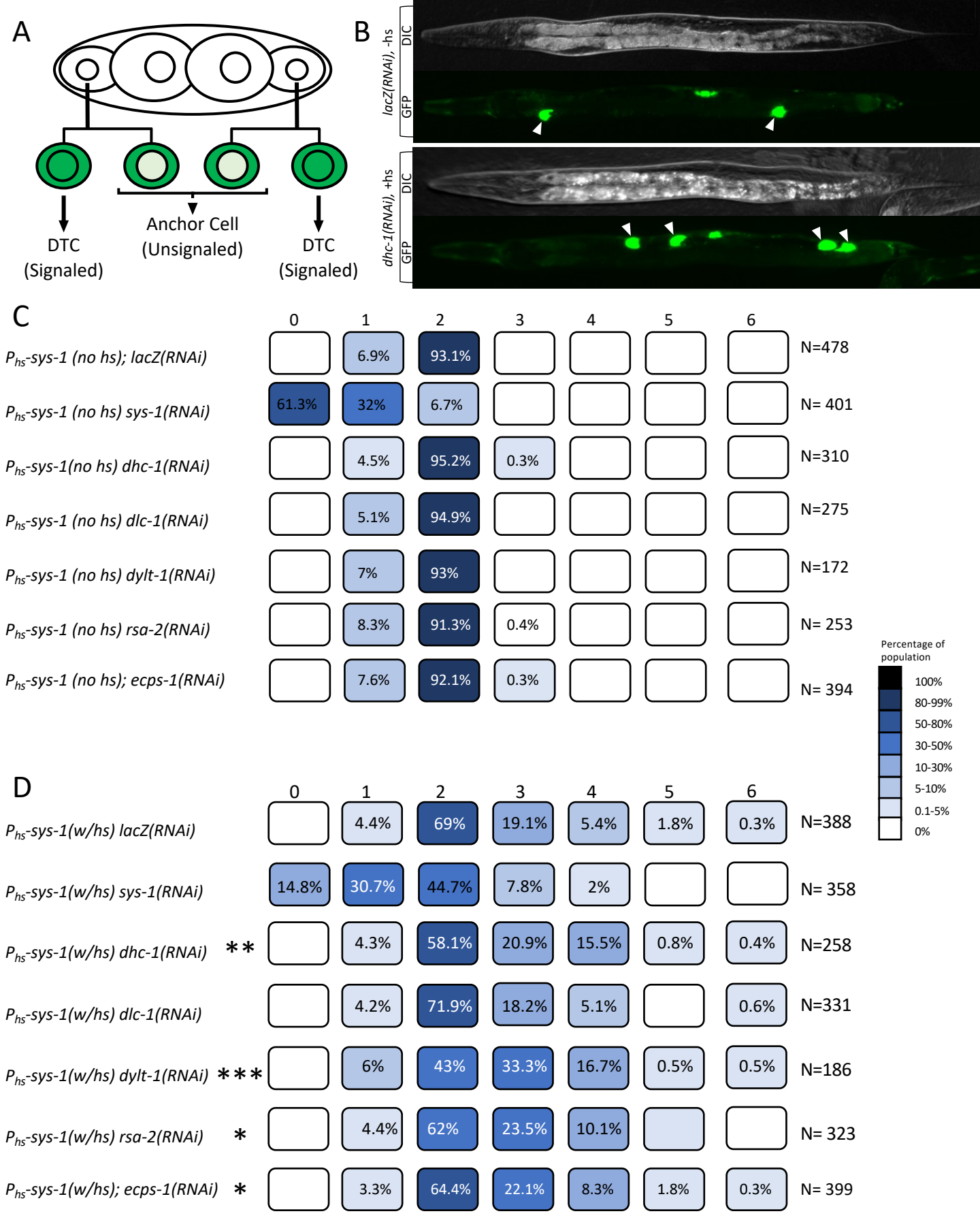
A
DTC
(Signaled)
Anchor Cell
(Unsignaled)
DTC
(Signaled)
B
lacZ(RNAi), -hs
DIC
GFP
dhc-1(RNAi), +hs
DIC
GFP
C
0 1 2 3 4 5 6
Phs-sys-1 (no hs); lacZ(RNAi) 6.9% 93.1% N=478
Phs-sys-1 (no hs) sys-1(RNAi) 61.3% 32% 6.7% N= 401
Phs-sys-1(no hs) dhc-1(RNAi) 4.5% 95.2% 0.3% N=310
Phs-sys-1 (no hs) dlc-1(RNAi) 5.1% 94.9% N=275
Phs-sys-1 (no hs) dylt-1(RNAi) 7% 93% N=172
Phs-sys-1 (no hs) rsa-2(RNAi) 8.3% 91.3% 0.4% N= 253
Phs-sys-1 (no hs); ecps-1(RNAi) 7.6% 92.1% 0.3% N= 394
Percentage of population
100%
80-99%
50-80%
30-50%
10-30%
5-10%
0.1-5%
0%
D
0 1 2 3 4 5 6
Phs-sys-1(w/hs) lacZ(RNAi) 4.4% 69% 19.1% 5.4% 1.8% 0.3% N=388
Phs-sys-1(w/hs) sys-1(RNAi) 14.8% 30.7% 44.7% 7.8% 2% N= 358
Phs-sys-1(w/hs) dhc-1(RNAi) ** 4.3% 58.1% 20.9% 15.5% 0.8% 0.4% N=258
Phs-sys-1(w/hs) dlc-1(RNAi) 4.2% 71.9% 18.2% 5.1% 0.6% N=331
Phs-sys-1(w/hs) dylt-1(RNAi) *** 6% 43% 33.3% 16.7% 0.5% 0.5% N=186
Phs-sys-1(w/hs) rsa-2(RNAi) * 4.4% 62% 23.5% 10.1% N= 323
Phs-sys-1(w/hs); ecps-1(RNAi) * 3.3% 64.4% 22.1% 8.3% 1.8% 0.3% N= 399

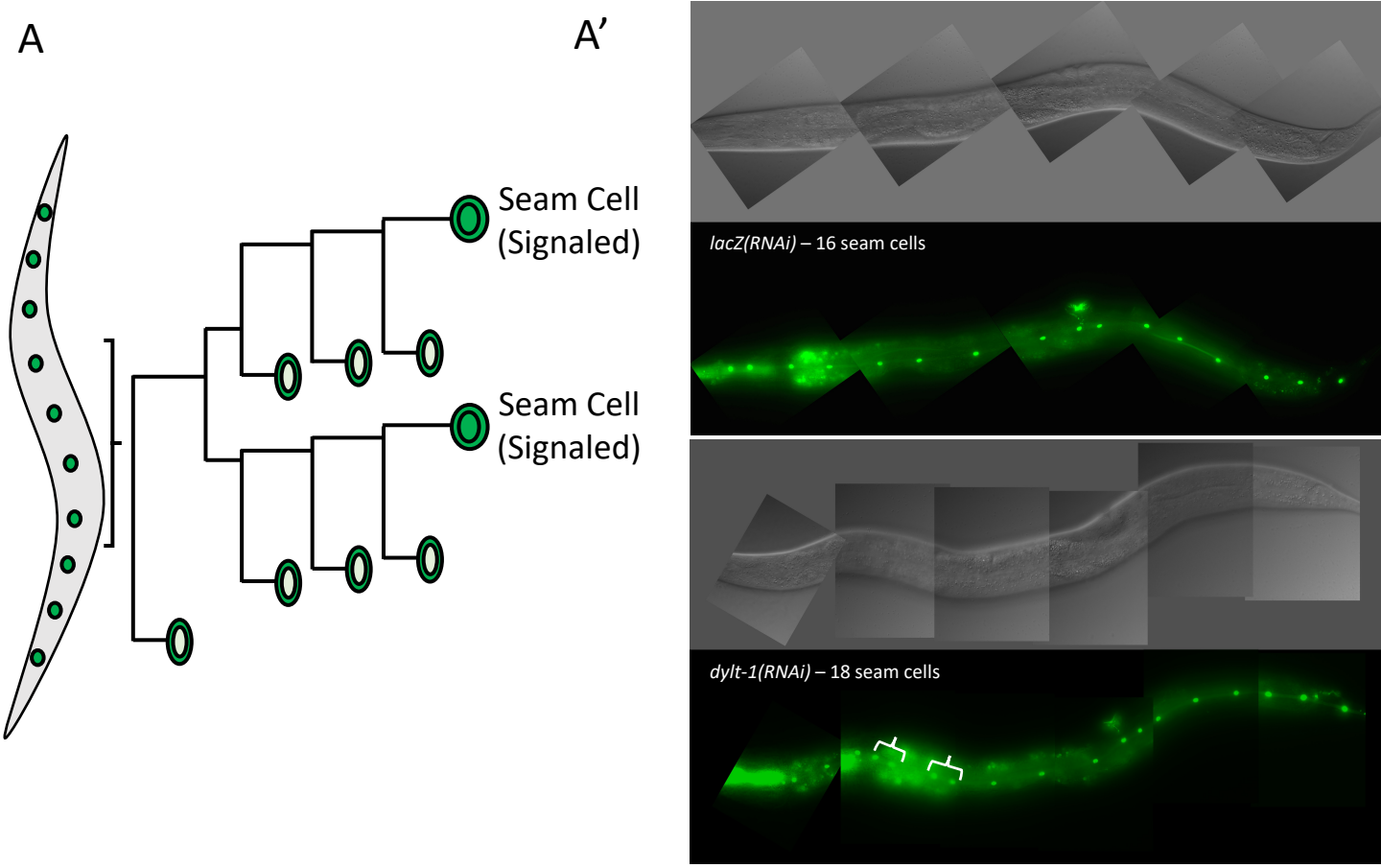

B

# of SCs		15	16	17	18	19	20	21	
P_{hs}-sys-1 (no hs); lacZ(RNAi)		1.7%	95%	3.3%					N=60
P_{hs}-sys-1 (no hs); dlc-1(RNAi)	*		90%	8.3%			1.7%		N= 60
P_{hs}-sys-1 (no hs); dylt-1(RNAi)	*		88.3%	10%			1.7%		N= 60

C

# of SCs		15	16	17	18	19	20	21	
P_{hs}-sys-1 (w/hs); lacZ(RNAi)		1.7%	80%	13.3%	5%				N=60
P_{hs}-sys-1 (w/hs); dlc-1(RNAi)	**	1.7%	58.3%	33.3%	5%	1.7%			N= 60
P_{hs}-sys-1 (w/hs); dylt-1(RNAi)	***	1.7%	38.2%	26.7%	11.7%	11.7%	5%	5%	N= 60

Percentage of population

- 100%
- 80-99%
- 50-80%
- 30-50%
- 10-30%
- 5-10%
- 0.1-5%
- 0%

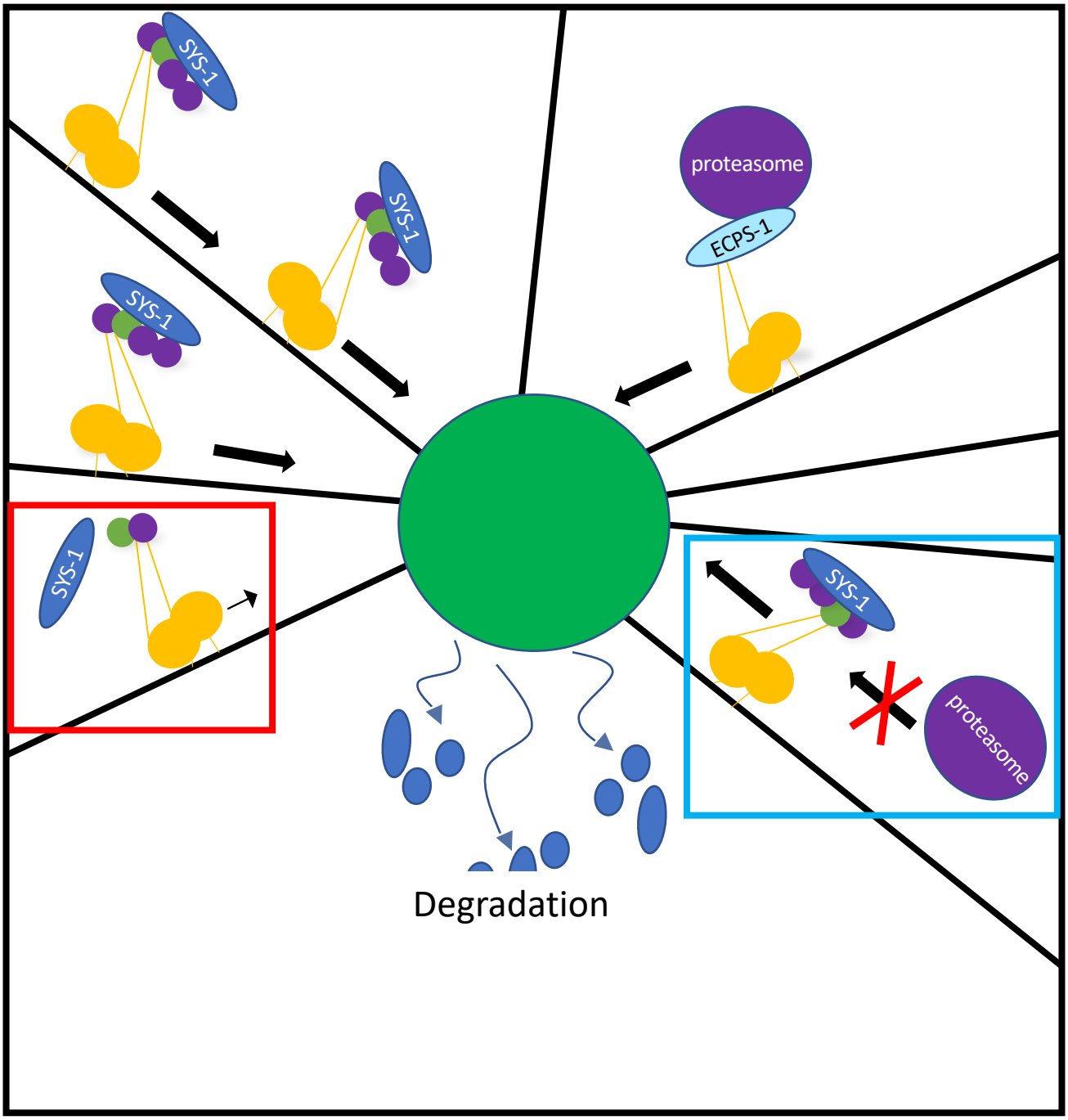
SYS-1
SYS-1
SYS-1
proteasome
ECPS-1
SYS-1
SYS-1
proteasome
Degradation